2014

Age and weathering rate of sediments in small catchments: the role of hillslope erosion

Anthony Dosseto
University of Wollongong, tonyd@uow.edu.au

Heather L. Buss
University of Bristol

Francois Chabaux
University of Strasbourg

Publication Details

Dosseto, A., Buss, H. L. & Chabaux, F. (2014). Age and weathering rate of sediments in small catchments: the role of hillslope erosion. Geochimica et Cosmochimica Acta, 132 238-258.

Age and weathering rate of sediments in small catchments: the role of hillslope erosion

Abstract
Uranium-series (U-series) isotopes in river material can be used to determine quantitative time constraints on the transfer of erosion products from source to sink. In this study, we investigate the U-series isotope composition of river-borne material in small catchments of Puerto Rico and southeastern Australia in order to improve our understanding of (i) the controls on the U-series isotope composition of river-borne material and (ii) how erosion products acquire their geochemical characteristics. In both regions, thorium isotopes track the origin of sediment and dissolved loads. Stream solutes are mainly derived from the deepest part of the weathering profile, whereas stream sediments originate from much shallower horizons, even in landslide-dominated Puerto Rican catchments. This suggests that in environments where thick weathering profiles have developed, solutes and sediments have distinct origins. The U-series isotope composition of stream sediments was modelled to infer a weathering age, i.e. the average time elapsed since the sediment's minerals have started weathering. In southeastern Australia, the weathering age of stream sediments ranges between 346 ± 12 kyr and 1.78 ± 0.16 Myr, similar to values inferred from weathering profiles in the same catchment. Old weathering ages likely reflect the shallow origin of sediments mobilised via near-surface soil transport, the main mechanism of erosion in this catchment. Contrastingly, in Puerto Rico weathering ages are much younger, ranging from 5.1 ± 0.1 to 19.4 ± 0.4 kyr, reflecting that sediments are derived from less weathered, deeper saprolite, mobilised by landslides. Weathering ages of stream sediments are used to infer catchment-wide, mineral-specific weathering rates that are one to two orders of magnitude faster for Puerto Rico than for southeastern Australia. Thus, the type of erosion (near-surface soil transport vs. landslide) also affects the weathering rate of river sediments, because their weathering ages determine the potential for further weathering during sediment transport and storage in alluvial plains.

Disciplines
Medicine and Health Sciences | Social and Behavioral Sciences

Publication Details
Dosseto, A., Buss, H. L. & Chabaux, F. (2014). Age and weathering rate of sediments in small catchments: the role of hillslope erosion. Geochimica et Cosmochimica Acta, 132 238-258.

Age and weathering rate of sediments in small catchments: the role of hillslope erosion

Anthony Dosseto[1,*], Heather L. Buss[2] and François Chabaux[3]

[1] Wollongong Isotope Geochronology Laboratory. School of Earth and Environmental Sciences, University of Wollongong. Wollongong, NSW 2522, Australia

[2] School of Earth Sciences, University of Bristol, Wills Memorial Building, Bristol, BS8 1RJ, UK

[3] Laboratoire d'Hydrologie et de Géochimie de Strasbourg (LHyGES), Université de Strasbourg et CNRS, 1 rue Blessig, 67084 Strasbourg Cedex, France

* Corresponding author: tonyd@uow.edu.au. Tel: +61 2-4221-4805; Fax: +61 2-4221-4250

Abstract

Uranium-series (U-series) isotopes in river material can be used to determine quantitative time constraints on the transfer of erosion products from source to sink. In this study, we investigate the U-series isotope composition of river-borne material in small catchments of Puerto Rico and southeastern Australia in order to improve our understanding of (i) the controls on the U-series isotope composition of river-borne material and (ii) how erosion products acquire their geochemical characteristics. In both regions, thorium isotopes track the origin of sediment and dissolved loads. Stream solutes are mainly derived from the deepest part of the weathering profile, whereas stream sediments originate from much shallower horizons, even in landslide-dominated Puerto Rican catchments. This suggests that in environments where thick weathering profiles have developed, solutes and sediments have distinct origins.

The U-series isotope composition of stream sediments was modelled to infer a weathering age, i.e. the average time elapsed since the sediment's minerals have started weathering. In southeastern Australia, the weathering age of stream sediments ranges between 346 ± 12 kyr and 1.78 ± 0.16 Myr, similar to values inferred from weathering profiles in the same catchment. Old weathering ages likely reflect the shallow origin of sediments mobilised via near-surface soil transport, the main mechanism of erosion in this catchment. Contrastingly, in Puerto Rico weathering ages are much younger, ranging from 5.1 ± 0.1 to 19.4 ± 0.4 kyr, reflecting that sediments are derived from less weathered, deeper saprolite, mobilised by landslides. Weathering ages of stream sediments are used to infer catchment-wide, mineral-specific weathering rates that are one to two orders of magnitude faster for Puerto Rico than

for southeastern Australia. Thus, the type of erosion (near-surface soil transport vs. landslide) also affects the weathering rate of river sediments, because their weathering ages determine the potential for further weathering during sediment transport and storage in alluvial plains.

Introduction

The measurement of uranium-series isotopes in river material can be used to determine time constraints on erosion and weathering processes (Chabaux et al., 2008; Chabaux et al., 2006; Chabaux et al., 2003b; DePaolo et al., 2006; Dosseto et al., 2006a; Dosseto et al., 2006b; Dosseto et al., 2008a; Dosseto et al., 2006c; Granet et al., 2010; Granet et al., 2007; Lee et al., 2010; Vigier and Bourdon, 2011; Vigier et al., 2005; Vigier et al., 2001; Vigier et al., 2006). One particularly important parameter to understand the dynamics of soil formation, erosion and sediment transfer at the catchment scale is the *weathering age* of soil and sediment as inferred from U-series isotopes (termed in previous studies "residence time" or "transport time"; Andersen et al., 2013; Chabaux et al., 2013; Chabaux et al., 2008; Chabaux et al., 2003a; Chabaux et al., 2006; Chabaux et al., 2003b; DePaolo et al., 2006; Dequincey et al., 1999; Dequincey et al., 2002; Dosseto et al., 2006a; Dosseto et al., 2006b; Dosseto et al., 2008a; Dosseto et al., 2011; Dosseto et al., 2012; Dosseto et al., 2010; Dosseto et al., 2006c; Granet et al., 2010; Granet et al., 2007; Keech et al., 2013; Lee et al., 2010; Ma et al., 2010; Pelt et al., 2008; Vigier and Bourdon, 2011; Vigier et al., 2005; Vigier et al., 2001; Vigier et al., 2006). This age represents the average amount of time elapsed since the minerals that compose the soil or sediment have started to chemically weather (i.e. the onset of mineral dissolution in the bedrock). The weathering age of sediments integrates both their storage in weathering profiles and transport in the river. Note that where the transport time in the river is short (e.g. little or no storage in an alluvial plain), the weathering age of sediments gives a catchment-averaged estimate of the age of weathering profiles (Fig. 1). Recent studies have shown that the

sediment weathering age can vary from as little as a few hundreds of years in Iceland (Vigier et al., 2006) to several hundreds of thousands of years in the lowlands of the Amazon basin (Dosseto et al., 2006a). Most of these studies have focused on large catchments: Amazon (Dosseto et al., 2006a; Dosseto et al., 2006b), Ganges (Granet et al., 2010; Granet et al., 2007), Mackenzie (Vigier et al., 2001), Murray-Darling (Dosseto et al., 2006c). In order to improve our understanding of the controls on the sediment weathering age, here we focus on small catchments draining granitic (Rio Sabana and Rio Icacos) and volcaniclastic lithologies (Rio Mameyes) in tropical Puerto Rico and granitic lithologies in temperate southeastern Australia (Nunnock River). These catchments were chosen because Rio Sabana and Icacos are underlain by similar parent rock as the Nunnock River but characterised by a much wetter and warmer climate, thus allowing us to study the role of climate on weathering age. Furthermore, the Rio Mameyes catchment has similar climatic features to Rio Sabana and Icacos catchments such that the role of lithology can be ascertained.

Study areas

Nunnock River basin, New South Wales, Australia

The Nunnock River is a tributary of the Bega River (southeastern Australia), which drains the eastern flank of the Great Dividing Range into the Tasman Sea (Fig. 2a). This relief formed as a result of the initiation of rifting that opened the Tasman Sea approximately 80 Ma ago (Ollier, 1982) and has been slowly propagating inland since then. Altitude ranges 1100 m at the source of the Nunnock River to 220 m at the confluence with the Bega River. The catchment is

92 underlain by the Palaeozic granodioritic Bemboka suite of the Bega batholith (White and
93 Chappell, 1983).

94 The Nunnock River catchment is vegetated by schlerophyl forest dominated by stringy
95 bark eucalyptus. Rain falls throughout the year and the mean annual precipitation is ~ 910
96 mm/yr (Bureau of Meteorology Australia, 1999). The average annual temperature is 10ºC
97 (Bureau of Meteorology Australia, 1999). Hillslope erosion is dominated by near-surface soil
98 transport, as illustrated by numerical modelling of hillslope sediment transport in this
99 catchment (Braun et al., 2001; Heimsath et al., 2002). This in agreement with Prosser et al.
100 (2003; 2001) who suggest that in this region near-surface soil erosion dominates over rill and
101 gully erosion. Furthermore, based on field and satellite imagery survey, no evidence for
102 landsliding was found. Field survey also suggests that there is no significant alluvium storage in
103 the Nunnock River catchment. Discharge has not been monitored and no measurement was
104 available at the time of sampling. The concentration of suspended sediments was measured at
105 the time of sampling and ranges from 2 to 12 mg/l. The river was sampled at five different
106 locations (Fig. 2a). Sample NUN01 was collected near the source of the river and integrates a
107 very small swamp area (~0.25 km^2). Samples NUN01, 02 and 03 were collected at sites where
108 the river only drains the plateau area, which covers ~18 km^2, while at NUN04 and 05 sample
109 sites the river drains both the plateau and the escarpment. At NUN05, the drainage area is ~33
110 km^2. About 5 to 10 litres were collected and filtered at 0.2 μm to separate the suspended
111 sediments from the dissolved+colloidal load. Bedload sediments were also sampled for the
112 three most downstream locations. The channel width at these locations was only ~1-2m and
113 the water height <1 m. Bedload sediments were collected across the river bed over ~10m of

114 channel length. These sediments are medium to coarse sands and are only expected to
115 experience significant transport during high discharge events. Two soil samples were collected
116 at 30 and 50 cm depth from a pit located on the same hillslope as the one studied in Dosseto et
117 al. (2008b).

118 ## Luquillo Mountains, Puerto Rico

119 The river basins studied are located in the Luquillo Experimental Forest (Luquillo
120 Mountains, eastern Puerto Rico; Fig. 2b). The Rio Icacos and Rio Sabana run from north to south
121 and are tributaries of the Rio Blanco, which drains into the Caribbean Sea on the southeast side
122 of the island. The Rio Mameyes runs south to north and discharges directly into the Atlantic
123 Ocean on the north side of the island.

124 Relief is characterized by steep slopes in all three catchments with elevation varying
125 between 616 and 844 m for Icacos above the stream gage, between 84 and 1040 m for
126 Mameyes above the stream gage at Puente Roto, and between 330 and 1024 m for Sabana,
127 which is not gauged. The Icacos and Sabana basins are underlain by the Rio Blanco quartz
128 diorite (49-42 Ma; Smith et al., 1998) which constitutes 99% of the lithology drained, whereas
129 the Rio Mameyes basin is mostly underlain by marine-deposited basaltic to andesitic
130 volcaniclastics of the Fajardo and Tabonuco Formations (both about 100 Ma; Jolly et al., 1998b),
131 with some quartz diorite and contact-metamorphosed volcaniclastics in the uppermost parts of
132 the catchment. The vegetation in the studied catchments is mostly subtropical to lower
133 montane rainforest, with dwarf forests at the highest elevations and Sierra Palm forests at
134 lower elevations. The Mameyes River basin is covered by lower montane rainforest dominated
135 by Tabonuco trees (*Dacryodes excelsa*) and the Icacos and Sabana River basins by lower

montane wet forest dominated by Colorado trees (*Cyrilla racemiflora*). Precipitation increases with elevation and ranges from 3530 to 4850 mm/yr with an average value of 4200 mm/yr in the Icacos basin and 3482 mm/y in the Mameyes basin (Heartsill-Scaley et al., 2007; White et al., 1998). Mean annual temperature is 22 °C. Mean monthly temperatures at lowest elevations range from about 23.5 °C in January to 27 °C in September, and at the highest elevations from 17 °C to 20 °C. Discharge is highly variable with very high discharge during rain events returning quickly to very low base flows after the events. Mean annual runoff for Rio Icacos is 3610 mm/yr with a drainage area of 3.26 km^2 (Peters et al., 2006). Mean annual runoff for Rio Mameyes is 2441 mm/yr with a drainage area of 17.8 km^2 (Larsen and Stallard, 2000). Rio Icacos mean annual sediment yield is 954 t/km^2 and the median annual sediment concentration is 27.7 mg/L (Larsen, 2012). Mameyes River mean annual sediment yield is 227 t/km^2 and the median annual sediment concentration is 12.8 mg/L (Larsen, 2012). Runoff and sediment yields have not been determined for the Sabana River. Landslides are the major erosion drivers in the Icacos and Mameyes basins, where they constitute 93% and 98% of the total hillslope erosion, respectively (Larsen, 2012). Landslides are twice more frequent in the Icacos basin compared to Mameyes, which is accounted for by the more erodible nature of the soil and saprolite derived from the quartz diorite (Larsen, 2012). Mean landslide depth ranges from 2 to 9 m for Icacos, and 2 to 12 m for Mameyes (Larsen, 2012). Mass balance on in-situ ^{10}Be concentrations in Icacos sediments suggest that, for the samples considered, 55% of the sediments are derived from mass wasting events (Brown et al., 1995). In both watersheds, fractured bedrock corestones are embedded in saprolite below about 5 m depth (Buss and White, 2012; Buss et

al., 2013; Buss et al., 2008), providing multiple weathering interfaces supplying freshly weathered sediments at depth.

Sampling was undertaken in July 2005 during base flow conditions. Water was filtered soon after collection (see "Analytical Techniques" section). Bedload sediments were collected from six streams. In all instances, bedload sediments were medium to coarse sands. For RI-2, RI-4 and RI-7, the stream width was <1 m and the water height <0.5 m, thus bedload samples were collected across the stream bed over a channel length of ~4 m. RI-7 "bank" sediments were collected from the side of the stream channel, above the water level. Similar aspect (grain size and mineral type) to RI-7 bed sediments suggests that the material sampled was not soil but indeed stream sediment. For RI-3 and RI-5, the channel width was 5-10 m and 2-4 m, respectively, and the water height <1.5 m; bed sediments were collected across the channel over a channel length of ~10-20 m. For RI-6, the channel width was 2-4 m and the water height <1 m; bed sediments were collected across the channel over a channel length of ~10 m. For samples RI-2 and RI-4, grain size of bedload sediments appeared finer (silt size) than for other sediment samples (based on field observations since grain size distribution was not measured). Parent rock samples were also collected from outcrops in both the Icacos and Mameyes catchments. Although the composition of the parent rock varies somewhat across the catchments (e.g., Buss et al., 2013; Jolly et al., 1998a; Turner et al., 2003), these samples are only used as an estimate of the composition of the parent material for comparison to that of erosion products. Regolith samples from the LG1 weathering profile studied in Buss et al. (2005; Buss et al., 2010), Pett-Ridge et al. (2009a; 2009b), Schulz and White (1999) and White et al. (1998), were also analysed.

Analytical techniques

For Puerto Rico, river water samples were processed at the US Geological Survey at Guaynabo (Puerto Rico) using two different techniques: (i) filtration at 0.2 μm using acetate cellulose filters in a PTFE enclosure. The filtered water, i.e. <0.2 μm fraction, was labelled "dissolved+colloidal load". The suspended load (i.e. >0.2 μm fraction) was recovered from the filter by rinsing it with 18 MΩ water, centrifuging the solution and discarding the supernatant, followed by drying at 80 °C in acid-washed PTFE containers. (ii) Filtration at 25 μm (cellulose mesh) followed by tangential filtration using a stack of membranes allowing successive filtrations at 0.2 μm, 100 kilo-daltons (kDa) and 10 kDa. Thus in the second procedure, we obtained two suspended load size fractions: >25 μm and 2-25 μm, two colloidal size fractions: 100 kDa - 0.2 μm, 10-100 kDa, and the dissolved load: <10 kDa. The size fraction >25 μm was collected by rinsing the mesh with 18 MΩ water, centrifuging the solution and discarding the supernatant, followed by drying at 80 °C in acid-washed PTFE containers. Colloidal fractions were dried down at 80 °C in acid-washed PTFE containers. For southeastern Australia, river water samples were filtered in the field at 0.2 μm as described above. At both study sites, the concentration of suspended matter was determined by filtering a known volume of water (generally 1L) and weighing the filter after drying. The error estimated on suspended matter concentrations is no more than 5-10 %.

Colloidal fractions, suspended, bedload sediments and regolith samples were homogenised and gently crushed in an agate mortar. Sediments and regolith were first dried at 100 °C to remove the water. The Loss-on-ignition (LOI) was determined at the Geochemical Analysis Unit (Macquarie University) by ashing a weighed amount of dry sample (~2g for each

sample) at 550 °C for 5 hours in a furnace. LOI is used as a proxy for soil organic content, as previously suggested in numerous studies (e.g. Bengtsson and Enell, 1986; Dean, 1974; Donkin, 1991; Goldin, 1987; Heiri et al., 2001; Spain et al., 1982), noting however that this parameter can also include dehydration of clay minerals and metal oxides (Heiri et al., 2001). Nevertheless, neglecting the role of clays on LOI values still accounts for 91 % of the variance between LOI and measured organic carbon content (Spain et al., 1982). Soil samples were processed at the Research School of Earth Sciences (Australian National University) to produce quartz separates, as commonly performed for in-situ cosmogenic isotope measurement, and following a procedure modified from (Kohl and Nishiizumi, 1992).

For Zr (and other trace elements) analyses, standard methods were employed (e.g. Eggins et al., 1997). Sample preparation was performed at the Geochemical Analysis Unit (Macquarie University). Approximately 100 mg of ground solid sample was weighed into clean 15 ml Savillex® PFA vials. Samples were digested using a 1:1 mixture of HF (Merck, Suprapur grade) and HNO_3 (Ajax) at 160 °C for 24 h, then dried down and repeated. The samples were then further digested in 6M HNO_3 for 24 h, dried down again, and diluted to 10 ml in 2% HNO_3 with trace HF. Then 1:1000 dilutions of each sample were individually spiked with a 15 µl aliquot of a solution of Li, As, Rh, In, Tm and Bi in 2% HNO_3. Samples and standards were analysed by quadrupole inductively coupled plasma mass spectrometry (ICP-MS) on an Agilent 7500 c/s system at the GAU, Macquarie University. BCR-2 was used as a calibration standard to correct for instrument sensitivity and run drift. The background was measured on a 2% HNO_3 rinse solution.

For Sr isotope determination, sample preparation was undertaken at the Geochemical Analysis Unit (Macquarie University). Purification of Sr was carried out using powders digested in PFA vials with concentrated HF and HNO_3. Samples were then dried down and ~1 ml of concentrated $HClO_4$ was added, followed by 4 ml 6M HCl and H_2O_2. These were dried down once again, dissolved in 6M HCl, dried, dissolved in HCl and HF, and centrifuged to check for the presence of any undissolved residue (none was observed). The samples were then loaded onto Teflon columns using Biorad® AG50W-X8 (200–400 mesh) cation exchange resin and eluted in 2.5N HCl–0.1N HF. Strontium isotopic analyses were obtained by thermal ionization mass spectrometry (TIMS) using a Thermo Finnigan Triton system at the GAU, Macquarie University, Sydney. Strontium was loaded onto single rhenium filaments with a Ta activator and analysed between 1380 and 1430 °C in a static measurement mode with rotating amplifiers. NIST SRM 987 was analysed for instrument sensitivity during times of the analyses (n = 17) and gave a long-term reproducibility of $^{87}Sr/^{86}Sr$ = 0.710250 (2SD = 0.000034). Ratios were normalized to $^{86}Sr/^{88}Sr$ = 0.1194 to correct for mass fractionation.

For U-series isotope determination, sample preparation and analysis were performed Geochemical Analysis Unit (Macquarie University). A tracer solution enriched in ^{236}U-^{229}Th and another tracer solution enriched in ^{228}Ra were added to the ground solid sample, in order to determine U, Th and ^{226}Ra concentrations, respectively (Tables 1 and 2). The masses of sample and ^{236}U-^{229}Th tracer solution were chosen to minimise its contribution on ^{234}U, ^{235}U, ^{238}U, ^{230}Th and ^{232}Th (<0.1 %) while yielding beams greater than 50,000 cps for ^{236}U and ^{229}Th. The masses of sample and ^{228}Ra tracer solution were optimised to yield a measured $^{228}Ra/^{226}Ra$ as close to 1 as possible. The mixture of sample and tracer solutions was then dissolved in $HClO_4$, HF and

244 HNO_3. Fluorides were driven off by evaporation at 100 °C followed by step evaporation at 150
245 °C, 170 °C and 200 °C. Samples were then taken up in 7M HNO_3 and centrifuged to check for the
246 presence of any undissolved residue (none was observed) before U-Th separation. For dissolved
247 and dissolved+colloidal load samples, about 30 mg of ^{236}U-^{229}Th solution and ~500 mg of ^{228}Ra
248 solution were added to ~300 g of <10 kDa fraction or to ~20 g of <0.2 μm fraction. This mixture
249 was left to equilibrate at room temperature for 3-5 days. It was then dried down at 100 °C and
250 re-dissolved in 7M HNO_3. U-Th were separated by ion chromatography using a BioRad™ AG1X8
251 anionic resin (yields >99 %; Dosseto et al., 2008b; Price et al., 2007). Ra was collected from the
252 U-Th column and processed through a series of two columns with BioRad™ AG50W-X8 cationic
253 resin and a last column with Eichrom Sr-SPEC resin (yields >99 %; Chabaux and Allègre, 1994). U
254 and Th isotopes were measured on a Nu Instruments Nu Plasma™ multi-collector ICP-MS
255 following procedures described in Sims et al. (2008). Briefly, mass bias and SEM/Faraday cup
256 yield were corrected by standard bracketing using CRM145 for U and Th"U" for Th. A linear
257 ^{232}Th tail correction was applied on ^{230}Th was measuring at masses 230.5 and 229.5. Ra was
258 measured by TIMS on a Thermo Scientific Triton™ following a procedure similar to that
259 described in Turner et al. (2000). Total procedure blanks were <10 pg for U and Th, and below
260 detection limit (~10 fg) for Ra. Accuracy was determined by measurement of the gravimetric
261 rock standard TML-3 (Table 1). U, Th and ^{226}Ra concentrations are within 1.2, 0.7 and 1.4 %,
262 respectively, of published values (Pietruszka et al., 2002; Sims et al., 2008) whilst ($^{234}U/^{238}U$),
263 ($^{230}Th/^{238}U$), ($^{226}Ra/^{230}Th$) and ($^{230}Th/^{232}Th$) ratios are within 0.6, 0.3, 0.4 and 0.1 % respectively,
264 of published values. In comparison, reproducibility of sample processing and analysis is poor,
265 probably reflecting heterogeneity in nuclide distribution: 6, 3 and 1% for Th, U and ^{226}Ra

concentrations, respectively; 5 and 3% for ($^{226}Ra/^{230}Th$) and ($^{230}Th/^{232}Th$) activity ratios (each replicate was measured on a different aliquot of sample that underwent the entire preparation separately). Nevertheless, reproducibility was much more satisfying for ($^{234}U/^{238}U$) and ($^{230}Th/^{238}U$) ratios: respectively 0.1 and 0.01%. Note that the poor reproducibility on concentrations and ($^{226}Ra/^{230}Th$) and ($^{230}Th/^{232}Th$) ratios does not affect our conclusions because the model used to calculate sediment weathering ages only considers ($^{234}U/^{238}U$) and ($^{230}Th/^{238}U$) ratios.

Results and Discussion

U-series isotope composition of river-borne material

Southeastern Australia

The U and Th concentrations in Nunnock River suspended sediments are higher than those in the bedrock (by a factor 1 to 3 for Th, 2 to 3 for U). This is consistent with the loss of more soluble elements, effectively concentrating U and Th in the suspended load. In contrast, the U, Th and ^{226}Ra concentrations in bedload sediments are about an order of magnitude lower than those in the suspended load. This can be explained if quartz (a U-Th-poor mineral phase) is abundant in the bedload, effectively "diluting" U, Th and ^{226}Ra concentrations by a factor of 10. Assuming that quartz contains no Th (or in the expected range of 10's of ppb; Table 1), a bedload composition of 80-97 wt. % quartz would be required to explain the difference in Th concentrations between suspended and bedload sediments. Considering a higher Th concentration in quartz and/or a significant proportion of quartz in the suspended load would only increase the required proportion of quartz in the bedload. Although the

287 calculated proportions of quartz are high, they are not unrealistic for bedload (see similar
288 calculations for Puerto Rico below).

289 In suspended sediments, U, Th and ^{226}Ra concentrations are positively correlated to the
290 Loss-on-ignition (LOI; Fig. 3). This suggests that the abundance of these elements in the
291 suspended load is controlled by adsorption onto organic particles or coatings (the LOI being
292 commonly used a proxy for organic matter; Bengtsson and Enell, 1986; Dean, 1974; Donkin,
293 1991; Goldin, 1987; Heiri et al., 2001; Spain et al., 1982). This relationship is not observed in
294 bedload sediments despite higher LOI values, suggesting that organic matter has little effect on
295 their U-Th-^{226}Ra budget.

296 Activity ratios for suspended sediments fall between values for bedload sediments and
297 dissolved+colloidal loads (Fig. 4). This is likely to reflect the contribution of secondary phases
298 precipitated with the isotopic composition of the stream water or the soil pore water. For
299 instance, (^{234}U/^{238}U) > 1 in suspended sediments is a common observation (see e.g. Chabaux et
300 al., 2008; Chabaux et al., 2003b; Dosseto et al., 2008a; Plater et al., 1992) and is generally
301 explained by an input of U during the precipitation of secondary phases from a solution with
302 (^{234}U/^{238}U) > 1. (^{234}U/^{238}U) less than 1 and (^{230}Th/^{238}U) greater than 1 in bedload sediments
303 follow the expected behaviour of ^{234}U, ^{238}U and ^{230}Th during weathering: depletion of ^{238}U over
304 ^{230}Th since U is generally more soluble than Th in oxidized conditions, and preferential loss of
305 ^{234}U over ^{238}U as a result of (i) direct recoil of ^{234}Th out of mineral grains and subsequent decay
306 into ^{234}U, (ii) preferential release of recoiled ^{234}U from crystal lattice damages (Fleischer, 1980,
307 1982a, b; Fleischer and Raabe, 1978; Hussain and Lal, 1986; Kigoshi, 1971). Ra is also expected
308 to be more soluble than Th because it is an alkali-earth and its behaviour is expected to follow

309 that of Ca or Mg, ($^{226}Ra/^{230}Th$) less than 1 should be found in stream sediments. However, the
310 opposite is observed. A possible explanation for ($^{226}Ra/^{230}Th$) >1 in sediments could be via the
311 deposition of dust with ($^{226}Ra/^{230}Th$) >1. This hypothesis has been invoked to account for ^{226}Ra
312 excesses in weathering profiles (Krishnaswami et al., 2004). However, Australian dust is
313 characterised ($^{226}Ra/^{230}Th$) <1 (Table A1; Marx et al., 2005) such that bulk deposition cannot
314 account for ratios greater than 1 in sediments. Alternatively, ^{226}Ra excesses could be explained
315 by the efficient adsorption of dissolved ^{226}Ra onto biotite (Ames et al., 1983b) and clays (Ames
316 et al., 1983a; Hidaka et al., 2007). Ames et al. have shown that (i) Ra can be adsorbed as soon as
317 it is released into solution (Ames et al., 1983a) and (ii) Ra is more efficiently adsorbed on
318 secondary minerals than U (Ames et al., 1983b). Thus, U-Th disequilibrium produced during
319 mineral dissolution could be relatively unaffected by adsorption while the associated Ra-Th
320 disequilibrium, ($^{226}Ra/^{230}Th$) <1, could be overprinted by Ra adsorption, resulting in ($^{226}Ra/^{230}Th$)
321 >1. If the ^{226}Ra excess in sediments is the result of ^{226}Ra uptake from solution, the
322 corresponding solution should have a ($^{226}Ra/^{230}Th$) <1. Since the stream dissolved load has a
323 ($^{226}Ra/^{230}Th$) greater than 1, the solution supplying Ra to sediments probably represents a small
324 fraction of the solute flux to the stream. Soil pore waters of the upper part of the weathering
325 profile could supply ^{226}Ra for adsorption since sediments are mostly derived from the upper
326 part of the profile whilst solutes originate from the deeper part (see below).
327
328 *Puerto Rico*
329 The U concentration of the parent rock sample for the Rio Icacos catchment is similar to
330 that of the quartz diorite as measured by Chabaux et al. (2013) on outcropping corestones in

331 the watershed, however the Th concentration is much lower (Table 2). These concentrations
332 are also lower than average values measured in the Rio Blanco quartz diorite by Smith et al.
333 (1998). This suggests that the parent rock sample analysed is not representative of the Rio
334 Blanco quartz diorite and may represent a magma of different composition. However, our
335 bedrock sample has a $^{87}Sr/^{86}Sr$ ratio (0.70433 ± 16) within error of that previously published for
336 the Rio Blanco quartz diorite (0.70413; Pett-Ridge et al., 2009b). Chabaux et al. (2013) have
337 noted that the Rio Blanco quartz diorite shows a wide range of textures and geochemical
338 compositions, as illustrated by the presence of finer-grained, more mafic xenoliths. Note that
339 the discrepancy between our measured U and Th concentrations and previously published data
340 does not affect our discussion since modelling of weathering ages is not based on U and Th
341 concentrations.

342 Th/U ratios in bedload and suspended sediments are greater than those measured in
343 the Rio Blanco quartz diorite (Smith et al., 1998). This suggests that sediments have
344 preferentially lost U during chemical weathering compared to Th. In contrast, U and Th
345 concentrations in suspended sediments are greater than in the bedrock or bedload sediments.
346 This concentration difference could be explained by a greater abundance of U,Th-rich
347 secondary minerals in finer size fractions or an enrichment in U,Th-poor minerals like quartz in
348 coarser size fractions. Note that in the second case, this would also imply that heavy minerals
349 like zircon are unlikely to be present in coarser sediments (where they are generally expected
350 to be concentrated) because this would result in higher U, Th concentrations in bedload
351 sediments. Assuming no Th in quartz (or 10's of ppb levels), 50-85% quartz in the >25 μm
352 fraction and 82-95% in the bedload are required to account for Th concentration differences

between the different sediment size fractions of Rio Icacos. Bedload in Rio Icacos contains ~90% quartz (Brown et al., 1995), consistent with our estimate. For Rio Sabana, which is also underlain by quartz diorite bedrock, these proportions are similar: 27-78% for the >25 μm fraction and 76-93% for the bedload. Calculations with U instead of Th yield similar estimates for both rivers.

In Icacos and Mameyes bedrock samples, ^{234}U-^{238}U is in secular equilibrium as expected. However, interestingly, ^{230}Th-^{238}U shows significant disequilibrium (Table 2). A ($^{230}Th/^{238}U$) ratio greater than 1 (Icacos bedrock) could indicate a recent loss of uranium during the early stages of water-rock interaction as the rock was recently exposed to meteoric waters. Conversely, a ($^{230}Th/^{238}U$) ratio less than 1 (Mameyes bedrock) suggests either a loss of Th or gain of U. What could induce either process is not well understood, however the very different ^{230}Th-^{238}U disequilibria in the Icacos and Mameyes bedrock samples suggest that, during the early stages of water-rock interaction, U-Th fractionation can be drastically different depending on the lithology.

As previously observed by Dosseto et al. (2006c) for the Murray-Darling river in Australia and Pogge von Strandmann (2011) in basaltic islands, there is a semi-continuous trend of activity ratios across size fractions (from <10 kDa dissolved loads to sand-sized bedload sediments; Fig. 5). Similar observations have been made for the Sr isotopic composition of colloidal and sediment size fractions (Douglas, 1993). To explain these variations, it was proposed that they reflect mixing between two components: on the one hand, detrital silicate grains (their abundance increasing with grain/colloid size) and on the other hand, natural organic matter and secondary minerals fingerprinting the isotopic composition of the solution.

As in Dosseto et al. (2006c), this hypothesis could also explain the U-series isotopic compositions observed in Figure 5 where an increasing contribution of detrital silicate grains with ($^{234}U/^{238}U$) ≤1 and ($^{230}Th/^{238}U$) ≥1 with colloid/sediment size, could account for the observed decrease in ($^{234}U/^{238}U$) and increase in ($^{230}Th/^{238}U$). In the same way, this model could also explain why suspended sediments in the Nunnock River have activity ratios intermediate to that of the dissolved+colloidal load and the bedload, since suspended sediments have a greater contribution of secondary minerals than the bedload.

Sediments show ($^{226}Ra/^{230}Th$) ratios both lower and greater than 1. Whilst ratios less than 1 are an expected product of the greater solubility of Ra over Th, ratios greater than 1 could be explained by adsorption of radium onto biotite, goethite and/or clays, as suggested above for Nunnock River sediments.

Lithological control on the U-series isotope composition of river-borne material

Because the catchments studied in Puerto Rico are characterized by nearly identical climatic conditions but underlain with different lithologies (quartz diorite for Icacos and Sabana; mostly volcaniclastics for Mameyes), we are able to investigate the effect of different parent material compositions on the U-series characteristics of river-borne material. Note however that only one sample was collected for Mameyes, thus it is difficult to argue that observations are unequivocally representative of the composition of river material for this catchment. Here we only attempt to identify strongly contrasting differences between Rio Mameyes, on the one hand, and Rio Icacos and Sabana, on the other hand.

Although the Rio Icacos and Nunnock Rivers are characterised by very different climatic conditions, the degree of U release from the granitic bedrock, as measured by the ratio of U concentration in the dissolved load over that in the bedrock, is similar for both catchments (1-3x10^{-5} for the Nunnock River, 0.8-1.8x10^{-5} for Rio Icacos). In contrast, the degree of U release from the volcaniclastic bedrock of Rio Mameyes is much lower (3.5-3.7x10^{-6}). This suggests that lithology has a much stronger role on dissolved U concentrations than climate. This could be explained by the difference in weathering susceptibility of the minerals dominating the U budget of sediments: biotite and hornblende for the Rio Blanco Formation quartz diorite (White et al., 1996), chlorite for the Fajardo Formation volcaniclastic rock (Buss et al., 2013).

Whilst Mameyes and Icacos/Sabana show similar (^{230}Th/^{238}U) ratios across the range of size fractions analysed, there is a strong contrast in ^{234}U-^{238}U disequilibrium in river-borne material between these two catchment groups. In the volcaniclastic catchment, sediments show a greater depletion in ^{234}U, and dissolved and colloidal fractions a greater ^{234}U enrichment, than in granitic catchments. The contrasting (^{234}U/^{238}U) ratios in river-borne material between the Mameyes and Icacos/Sabana catchments could be explained by a difference in the surface properties of sediments exported from each basin: the parental material in the Mameyes catchment is a fine-grained volcaniclastic rock, thus likely to produce sediments with a greater surface area than those of Rio Icacos/Sabana. A high surface area promotes the loss of ^{234}U during recoil, which would account for larger ^{234}U depletions in sediments and enrichments in waters.

Tracking solutes and sediments back to the weathering profile

Thorium isotopes are unlikely to fractionate during chemical weathering. Although ^{230}Th can be preferentially lost by recoil during radioactive decay of its parent, ^{234}U, or leaching of recoil tracks in which it is embedded, ^{230}Th is rapidly re-adsorbed on the sediment surface because of its high reactivity with particles (e.g. Plater et al., 1992). Moreover, because the half-life of ^{230}Th is 75.6 kyr (Cheng et al., 2013), U-Th fractionation during solute and sediment transport in the river will only modify their ($^{230}Th/^{232}Th$) ratio if the transport time in the fluvial system is longer than a few 10's of kyr. As it can be safely assumed that this is not the case for the catchments considered (because of the absence of contribution from old groundwater and the lack of significant alluvial deposits), the ($^{230}Th/^{232}Th$) ratio of solutes and sediments could be potentially used as a tracer of their origin.

For the Nunnock River, both bedload and suspended sediments have ($^{230}Th/^{232}Th$) similar to that in soils from the same catchment, but higher than saprolite values (Fig. 4c; Dosseto et al., 2008b). Conversely, in the dissolved load, ($^{230}Th/^{232}Th$) ratios are lower and less variable, ranging between 0.457 and 0.466, comparable to saprolite values (Fig. 4c). This suggests that stream sediments (both bedload and suspended load) are derived from the uppermost soil horizons (consistent with physical erosion dominated by near-surface soil transport in this catchment) whereas the dissolved load originates from the deeper parts of the weathering profile.

In Puerto Rico, ($^{230}Th/^{232}Th$) ratios increase systematically with size fraction (Fig. 5e). In comparison, in the LG1 weathering profile (located in the Rio Icacos catchment), ($^{230}Th/^{232}Th$) ratios increase with decreasing depth, from the saprock (mean = 0.952 ± 0.012, weighted 2

standard error; n = 6), through the saprolite (1.460 ± 0.14; n = 10) to the soil (1.775 ± 0.024; n = 5) (Table A2 and Fig. A2). Note that all three means are statistically different (t-test, p=0.05). Thus, similar to the Nunnock River, high ($^{230}Th/^{232}Th$) in Rio Icacos sediments (1.4-2.1) could indicate that they are derived from the upper horizons of weathering profiles whereas lower ($^{230}Th/^{232}Th$) ratios in colloidal and dissolved loads (1-1.2) could suggest that solutes and colloids originate from the lowermost horizons. This is consistent with previous studies in the Rio Icacos basin which have shown that most chemical weathering (thus solute production) takes place in the saprock (Buss et al., 2008; Pett-Ridge et al., 2009b; White et al., 1998). Kurtz et al. (2011) used Ge/Si ratios to determine that solutes in the Rio Icacos derive largely from the saprock and rock fractures during baseflow and from shallow soil and overland flow during stormflow.

The Sr isotopic composition of Icacos/Sabana stream sediments varies between 0.70471 and 0.70561 (Table 2). Pett-Ridge et al. (2009b) have shown that $^{87}Sr/^{86}Sr$ ratios decrease approximately linearly with increasing depth in the LG1 weathering profile, from values >0.710 in the topsoil to ~0.704 in the saprock (depth >5m). Thus, it is possible to reconcile the low Sr and high Th isotopic composition of stream sediments if they originate from intermediate depths of the weathering profile (4-5m). It is not implied that stream sediments derive exclusively from this horizon, but instead suggests that the sediment budget is dominated by material from the relatively deep saprolite. Because we are focusing on bedload sediments, it is possible that finer-grained material from the upper horizons was washed away preferentially by hydrodynamic sorting. The deep origin of stream sediments is not surprising since landslides 2-

12 m deep are the main mechanism for hillslope erosion in the Luquillo Mountains (Larsen, 2012; Larsen and Torres-Sánchez, 1992).

Although the origin of Rio Mameyes sediments is difficult to assess because there is no systematic ($^{230}Th/^{232}Th$) variation in the only weathering profile in this catchment studied for U-series isotopes (Dosseto et al., 2012), the ($^{230}Th/^{232}Th$) of the dissolved and colloidal fractions (1.64 ± 0.08) is similar to that of the bedrock sample analysed (1.754 ± 0.005). This would suggest that the relatively deep origin of solutes applies not only to different climatic environments (i.e. Puerto Rico vs. southeastern Australia) but also different lithologies. However, this hypothesis needs verification by further analyses of dissolved loads and bedrock of this catchment.

In summary, stream solutes and sediments have very distinct origins. On the one hand, solutes are derived from the deeper parts of the weathering profile, where minerals which dissolve readily have not yet been entirely consumed. On the other hand, sediments are derived from shallower horizons, from depths that depend on the mechanism of erosion (shallow depths where near-surface soil transport dominates like in the Nunnock River; deeper depths where landslides prevail like in the Rio Icacos). While these observations may not reflect global solute fluxes, considering the small size of the studied catchments, they seem valid regardless of climatic conditions (at least in tropical and temperate environments), and possibly for different lithologies. Thus, in slowly eroding environments where thick weathering profiles develop, not only do solute and sediment transport operate on different timescales, but they also are characterised by distinct spatial origins. Previous studies have used the geochemical composition of dissolved and sediment loads to assess whether erosion is in steady-state in a

481 catchment, i.e. whether the flux of solute and sediment exported is balanced by the flux
482 produced by bedrock weathering (Bouchez et al., 2011; Dosseto et al., 2006a; Dosseto et al.,
483 2006b; Dosseto et al., 2008a; Dosseto et al., 2006c; Gaillardet et al., 1995; Gaillardet et al.,
484 1997). However, these approaches assume that solutes and sediments have the same origin.
485 Our results suggest that this assumption might not be valid for catchments where thick
486 weathering profiles are present.

487 Quantification of the sediment weathering age

488 As explained above, it is possible to use the U-series isotope composition of river-borne
489 material to determine the weathering age of sediments (Fig. 1; Chabaux et al., 2008; Chabaux
490 et al., 2003b; Dosseto et al., 2008a; Vigier et al., 2001). We use the model of Dosseto et al.
491 (2008b) modified from (Dequincey et al., 2002), that describes the time evolution of a nuclide *j*
492 abundance in the sediments, N_j (in number of atoms), as follows (see also Chabaux et al.,
493 2013; Dosseto et al., 2012):

494 $$\frac{dN_j}{dt} = \lambda_i N_i - \lambda_j N_j + \Gamma_j N_{j,0} - w_j N_j \quad (1)$$

495 where N_i is the abundance of the parent nuclide i (in number of atoms), λ_i and λ_j are the
496 decay constants for nuclides i and j respectively (in yr^{-1}), Γ_j is the input constant (in yr^{-1})
497 representing the gain of nuclide *j* for instance by precipitation of secondary minerals from the
498 solution or by aeolian input, $N_{j,0}$ is the initial abundance of nuclide *j* in the bedrock (i.e. at time
499 = 0, the onset of bedrock weathering) and w_j is the dissolution constant for nuclide *j*. Examples
500 of evolution curves are shown on Fig. 6.

This equation can be written for ^{238}U, ^{234}U and ^{230}Th (note the first term of the right side of Equation (1) disappears for ^{238}U since it has no parent nuclide). The weathering age, T_w, is defined as the duration of continuous loss and gain of nuclides to evolve from the bedrock composition to the observed composition in sediments. In the model, the following assumptions are made:

- The bedrock is in secular equilibrium. If the age of the bedrock is greater than 1 Myr, this assumption is verified. The observation of activity ratios ≠ 1 in a rock older than 1 Myr simply indicates it has undergone water-rock interaction. This could imply that the U-series isotopic "clock" starts at a depth greater than the rock-regolith boundary. If this is the case, calculated weathering ages should be taken as maximum values;
- For a given set of samples, common Γ and w values apply and the difference in activity ratio between each sample is the result of different weathering ages. This implies that conditions for gain and loss of nuclides are similar across the set of samples considered. This assumption is reasonable for weathering profiles and small catchments but could be problematic for large catchments. However, it has been shown that there is a good correlation between weathering ages (calculated with the same approach) and independent indices of chemical weathering at the scale of the Rio Madeira basin in South America (a major tributary of the Amazon River), suggesting that this assumption may still be valid at the regional scale (Dosseto et al., 2006b);
- The coefficients for nuclide loss, w, and gain, Γ, are constant over the duration of weathering. This assumption is commonly made in studies modelling chemical weathering (e.g. Chamberlain et al., 2005; Ferrier and Kirchner, 2008) and laboratory

523 experiments suggest constant *w* values for a given mineral (White and Brantley, 2003).
524 Moreover, this is a reasonable assumption considering that dissolution and input
525 constants are likely to be similar at the small scale of the studied catchments, and
526 climatic variations have not been extreme over the past 10's of thousands of years in
527 the areas investigated. Even if spatial and temporal variations were significant, the
528 values calculated provide average estimates for each nuclide over T_w.

529 Only ($^{234}U/^{238}U$) and ($^{230}Th/^{238}U$) ratios in sediments are used to calculate weathering
530 ages. Thus, the number of known parameters in the model is 2*n*, where *n* is the number of
531 samples (i.e. ($^{234}U/^{238}U$) and ($^{230}Th/^{238}U$) ratios for each sample). The number of unknown
532 parameters is *n*+6, one Γ and one *w* value for each of the three nuclides considered and one
533 weathering age for each sample. If the number of samples considered is such that there are
534 more unknown parameters than known, further assumptions need to be made in order to
535 reduce the number of unknowns. The model is solved by minimising the sum of the squared
536 differences between the observed activity ratios and the activity ratios calculated with a
537 random set of Γ, *w* and T_w values. The minimisation is performed using the genetic algorithm
538 function in Matlab™. Variables are allowed to take values within a set range shown in Table A3.
539 A large number of solution sets is generated (>1,000) and the solution retained is the median of
540 this population. The error on solution parameters is calculated as the standard deviation of the
541 population of solutions.

542 For Rio Icacos/Sabana catchments, we considered 5 bedload sediment samples,
543 excluding RI-2 which shows a ($^{230}Th/^{238}U$) <1 unlike other samples from these catchments. We
544 used bedload sediment compositions as they are the least affected by secondary mineral

precipitation and their coarse grain size (typically fine sand) minimizes the contribution of aeolian material (Dosseto et al., 2006c). Note that the composition of Rio Mameyes sediments was not used in the model since it is shown above that U-series isotope fractionation differs significantly from that in the Rio Icacos/Sabana catchments (most likely as a result of contrasting parent rock lithologies). In order to have as many unknown as known parameters, ^{230}Th dissolution is assumed to be negligible (w_{230}/w_{234} = 10^{-10}), which is often the case (Chabaux et al., 2008; Dosseto et al., 2008a). Results are presented in Table 3. Weathering ages vary between 5 and 20 kyr, except for RI-4 which shows a much older age of 170 kyr. This older age could be explained if colluvium was sampled instead of stream sediments: at this sampling location, it was difficult to confidently assess whether a stream was sampled or in fact a gully cutting into the hillslope. These weathering ages are somewhat younger than the regolith residence times of 27-109 kyr calculated by Ferrier et al. (2010). The dissolution constant for ^{238}U is 4.7x10^{-6} yr^{-1}, which is similar to the values inferred for other tropical watersheds: Amazon lowlands: 4.4x10^{-6} yr^{-1} (Dosseto et al., 2006a); Ganges: 0.8-7x10^{-6} yr^{-1} (Granet et al., 2007) and Narmada-Tapti: 6.9-9.9x10^{-6} yr^{-1} (Vigier et al., 2005). The input constant for ^{238}U is similar to the dissolution constant, with a Γ_{238}/w_{238} of 0.5, suggesting that secondary mineral precipitation and/or aeolian input may be significant processes, at least for the U budget, even for coarse bedload sediments. This is in agreement with the findings in Pett-Ridge et al. (2009b), where a high dust flux was estimated for the Rio Icacos catchment (210 ± 70 kg ha^{-1} y^{-1}, based on a Sr isotope mass balance). The ratios of ^{234}U to ^{238}U dissolution constants, w_{234}/w_{238}, and input constants, $\Gamma_{234}/\Gamma_{238}$, are 1.095 and 1.128, respectively, which are similar to values commonly expected for natural environments (Dequincey et al., 2002).

We also considered a second scenario where the ^{230}Th dissolution constant is equal to that of ^{234}U, instead of being negligible. Results show that weathering ages are similar to those calculated in the first scenario assuming no ^{230}Th loss (except for RI-4; Table 3). The w_{234}/w_{238} and $\Gamma_{234}/\Gamma_{238}$ ratios are very similar between the two scenarios, whilst w_{238} and Γ_{238}/w_{238} show some variability. The main difference is the significant gain of ^{230}Th in the second scenario. Note that results are surprisingly consistent, considering the extreme nature of the two scenarios investigated.

For the Nunnock River, because only 3 bedload sediment samples were available, we solved the model for suspended sediments (5 samples). In this case, a value for w_{230} must be assumed such that the model is not under-constrained. Previous studies have shown that the dissolution constant for ^{230}Th is generally negligible (e.g. Vigier et al., 2005; Vigier et al., 2001) and we set w_{230} to be 10^{-10} smaller than w_{234} (i.e. $w_{230}/w_{234} = 10^{-10}$). Results are shown in Table 4. Weathering ages range from 443 kyr to 1.8 Myr. Interestingly, these values are similar to those inferred for weathering profiles from the same catchment (550 kyr to 6.2 Myr; Dosseto et al., 2008b). Moreover, considering an average weathering profile thickness of 20-30 m (Green et al., 2006), we can use denudation rates of 7-53 mm/kyr determined in (Heimsath et al., 2000) to calculate weathering ages ranging from 377 kyr to 4.3 Myr, similar to those inferred from U-series. A corollary of this comparison is that the weathering age is largely dominated by storage in weathering profiles. This is consistent with the lack of field evidence for significant alluvial storage. The calculated ^{238}U dissolution constant is 1.60 ± 0.04 x10^{-5} yr^{-1} (Table 4). This is intermediate to the values determined for saprolite (0.014-0.07 x10^{-5} yr^{-1}) and soil samples (10-74 x10^{-5} yr^{-1}) in Dosseto et al. (2008b). Calculated ratios of ^{234}U to ^{238}U

589 dissolution (w_{234}/w_{238}) and input constants ($\Gamma_{234}/\Gamma_{238}$) are 1.114 ± 0.003 and 1.083 ± 0.004,
590 respectively, similar to values obtained for Puerto Rico and commonly expected for natural
591 systems. Finally, the gain of ^{230}Th is negligible, with a calculated Γ_{230} of 1.7±0.4 x10^{-15} yr^{-1}.
592 Dosseto et al. (2008b) have shown that for weathering profiles in the Nunnock River catchment,
593 ^{230}Th gain and loss could actually be significant. Consequently, we considered a second scenario
594 where w_{230}/w_{234} is set to 0.5 (any values above 0.5 did not yield satisfying fit of the data).
595 Results show that although there can be significant differences in weathering ages for a given
596 sample, the range of values (350 kyr – 1.4 Myr) is similar to that calculated in the first scenario,
597 assuming no Th mobility (Table 4). Moreover, input and dissolution constants for ^{238}U and ^{234}U
598 are also comparable, the main difference being the significant gain of ^{230}Th in the second
599 scenario.

600 Although the model is poorly constrained for Nunnock River bedload sediments (only 6
601 known parameters), we performed calculations for different scenarios shown in Table 4.
602 Inferred weathering ages for bedload sediments (from 380 to 480 kyr) are intermediate to
603 those calculated for the suspended load. The dissolution constant for ^{238}U is similar to that
604 calculated for suspended sediments, whilst the input constant can vary extensively depending
605 on the scenario considered. The ratio of ^{234}U to ^{238}U input coefficients, $\Gamma_{234}/\Gamma_{238}$ reflects the
606 ^{234}U-^{238}U composition of the component supplying U to sediments. In bedload sediments, the
607 $\Gamma_{234}/\Gamma_{238}$ ratio is less than 1 and could be explained by the contribution of aeolian material
608 with (^{234}U/^{238}U) <1. In suspended sediments, dust contribution could be overprinted by the gain
609 of U with (^{234}U/^{238}U) >1 from metal oxides and organic matter coatings, resulting in an overall
610 modelled $\Gamma_{234}/\Gamma_{238}$ >1 for suspended sediments.

Catchment-wide weathering rates

Weathering ages as short as 5 kyr for Puerto Rico are surprising considering that weathering profiles in the Rio Icacos basin are several meters thick (White et al., 1998). Considering a minimum regolith thickness of 3 m (White et al., 1998), such a young age would imply a minimum erosion rate of 600 mm/kyr, which would be much greater than previous estimates using cosmogenic isotopes of ~43 mm/kyr (Brown et al., 1995) or 100 ± 23 mm/kyr (from amalgamated soil samples; Riebe et al., 2003). Moreover, weathering ages calculated here are somewhat younger than regolith residence times inferred in Ferrier et al. (2010). Young weathering ages suggest that stream sediments "bypass" the weathering profile and are instead removed directly from the deeper horizons, having undergone less chemical weathering (Fig. 1c). This scenario is plausible in Puerto Rico where hillslope erosion is strongly dominated by landslides with a mean depth between 2 and 12 m (Larsen, 2012). In contrast, older weathering ages calculated for the Nunnock River catchment reflect removal of sediment only from the top of old weathering profiles via near-surface soil transport (Fig. 1b).

An alternative hypothesis to explain older weathering ages for the Nunnock river would be to consider that weathering age is related to catchment size, where a larger catchment would imply a longer sediment transport time and thus a longer duration of weathering. Although the Nunnock River catchment is about ten times larger than Rio Icacos, there is no evidence for significant alluvial storage in either of these catchments that could justify such a relationship.

Yoo and Mudd (2008), building on work by White and Brantley (2003), proposed a law for the ground surface area-normalised weathering rate of minerals in regolith that combines mineral dissolution rate constants with weathering duration:

$$w_j = \frac{6 a_j b_j \omega_j}{D_j \rho_{\mu,j}} \tau_j^{\alpha_j + \beta_j} m_j \quad (2)$$

where subscript *j* refers to the mineral of interest, w_j is the weathering rate (in kg/m^2/yr), ω_j the molar mass (in mol/kg), D_j the particle diameter (in m), $\rho_{\mu,j}$ the density (in kg/m^3), m_j the present mass of mineral *j* per ground surface area (in kg/m^2) and τ_j is the amount of time mineral *j* has been exposed to weathering, i.e. the weathering age of mineral *j*. The constants *a*, *b*, α and β describe the relationship between the mineral dissolution rate constant, *R*, the mineral surface roughness, λ, and time: $R = a\tau^{\alpha}$ and $\lambda = b\tau^{\beta}$. The evolution of the mass of mineral j is described by the following equation:

$$m_j = m_{j,0} \exp\left[-\frac{6 a_j b_j \omega_j}{D_j \rho_{\mu,j} \left(1 + \alpha_j + \beta_j\right)} \tau_j^{1+\alpha_j+\beta_j} \right] \quad (3)$$

where $m_{j,0}$ is the initial mass of mineral *j* per ground surface area (in kg/m^2). It is calculated as $m_{j,0} = X_{j,0} \rho_r h$, where $X_{j,0}$ is the initial mass fraction of mineral *j* (in kg/kg), ρ_r is the density of the parent rock and *h* is the weathering profile thickness.

Equations 2 and 3 can be used to estimate catchment-wide weathering rates for specific minerals from the average weathering ages determined from U-series isotopes in sediments (this study) and values for the other parameters from the literature (Table 5; Buss et al., 2008; Ferrier et al., 2010; Murphy et al., 1998; White and Brantley, 2003; Yoo and Mudd, 2008). For Rio Icacos, using weathering ages between 5 and 20 kyr, we calculate catchment-wide biotite

652 weathering rates between 1.8x10^{-9} and 0.91x10^{-9} mol/m^2/s. In a previous study, Murphy et al.
653 (1998) have calculated biotite weathering rates from pore water Mg and K concentrations in a
654 regolith profile of Rio Icacos. These weathering rates, $w_{BET,j}$, were normalised to mineral surface
655 area (measured by the N_2 Brunauer-Emmett-Teller, BET, method). They can be compared to our
656 catchment-wide estimates by converting $w_{BET,j}$ values to ground surface area-normalised rates:

657 $$w_j^{'} = w_{BET,j} \frac{6\lambda m_j}{D\rho_{\mu,j}} \quad (4)$$

658 The resulting biotite dissolution rate, $w_j^{'}$, is 0.63x10^{-9} mol/m^2/s, which is slightly lower but
659 comparable to our estimates.

660 Catchment-wide weathering rates can also be determined for other minerals with our
661 approach. For plagioclase, we infer values ranging from 7.0x10^{-9} to 13x10^{-9} mol/m^2/s. These
662 rates are similar to those calculated from cosmogenic nuclides and mineral abundances: Ferrier
663 et al. (2010) reported a plagioclase weathering rate of 9.8x10^{-9} mol/m^2/s for Rio Icacos saprolite
664 (at 2.2 m depth) whilst Buss et al. (2008) calculated a faster rate of 27x10^{-9} mol/m^2/s for the Rio
665 Icacos saprock (converted from a BET surface area-normalised rate using Equation 4, assuming
666 a 5 kyr weathering age and a 0.5 m profile thickness representing the thickness of the saprock
667 layer analysed).

668 As anticipated because of older weathering ages, calculated plagioclase weathering
669 rates for the Nunnock river are slower than for Rio Icacos: between 0.075x10^{-9} and 0.78x10^{-9}
670 mol/m^2/s (calculated for weathering ages between 350 and 1800 kyr). This is similar to
671 weathering rates estimated for a hillslope in this catchment by Green et al. (2006): 0.7 – 2.5x10^{-}
672 ^{9} mol/m^2/s). A similar relationship between the two field sites is seen when comparing biotite

673 weathering rates, which are also much slower for the Nunnock River: 0.015×10^{-9} to 0.2×10^{-9}
674 $mol/m^2/s$.

675 When considering the parameters in Equations (2) and (3), the differences in mineral
676 weathering rates between southeastern Australia and Puerto Rico are largely driven by the
677 weathering age, which in turn is controlled by the type of erosion operating in each catchment.
678 The difference in mineral weathering rates between the two catchments is actually dampened
679 by the three-fold difference in weathering profile thickness: ~9 m for Rio Icacos (White et al.,
680 1998); ~30m for Nunnock River (Green et al., 2006). Taking into account the climatic setting of
681 both areas would further amplify differences in weathering rates since the Nunnock River
682 catchment is characterised by lower average temperatures and annual rainfall than the Rio
683 Icacos, such that the value of constant *a* in Equations 2 and 3 should be lower for the Nunnock
684 River.

685 Although it is shown here that solutes mainly originate from the deeper parts of the
686 weathering profiles (and thus where most of weathering takes place), *sediment* weathering
687 ages determine how much (and how fast) additional chemical weathering (and associated CO_2
688 consumption) can take place during sediment transport and storage in alluvial plains. Recently
689 it has been suggested that, at a global scale, weathering fluxes are dominated by sediment
690 weathering in alluvial plains (Lupker et al., 2012), although the importance of weathering during
691 sediment transport is debated (Bouchez et al., 2012). Dixon et al. (2009) have observed that at
692 the scale of the weathering profile, soils derived from extensively weathered saprolite would
693 undergo little additional weathering. Here, similar observations are made at the catchment
694 scale: the calculations above show that the type of erosion that operates in a catchment (e.g.

near-surface soil transport vs. landslides) exerts a dominant control on the weathering rates measured in sediments, accounting for differences of up to 2 orders of magnitude and thus setting the stage for further weathering during sediment transport and storage in alluvial plains.

Conclusions

The application of U-series isotopes to river-borne material in two small granitic catchments allows quantitative constraint of the origin of erosion products and their transit times through the catchment, the latter reflecting different modes of erosion. Th isotopes in river-borne material document the origin of stream solutes and sediments, in a similar manner to the use of U isotopes to identify water sources (Andersen et al., 2013; Andersson et al., 1995; Borole et al., 1982; Grzymko et al., 2007; Kraemer and Brabets, 2012; Porcelli et al., 2001; Riotte and Chabaux, 1999; Sarin et al., 1990). Both in the Nunnock River catchment and in Puerto Rico we find that sediments are mainly derived from the upper-intermediate parts of the weathering profile whilst solutes originate from the deeper parts, in agreement with previous findings for Puerto Rico (Buss et al., 2008; Ferrier et al., 2010; Kurtz et al., 2011; Turner et al., 2003; White et al., 1998).

The U-series isotope composition of river-borne material varies continuously between size fractions (dissolved, colloidal loads, suspended sediments and bedload), as previously observed for the Murray-Darling River basin (Dosseto et al., 2006c) and volcanic islands (Pogge von Strandmann et al., 2011). This observation is now generalized to catchments in various climatic settings and illustrates that the composition of erosion products carried by the river is a

716 mixture between detrital silicate grains on the one hand, and organic matter and secondary
717 minerals that fingerprint the composition of the solution on the other hand.

718 The weathering age of stream sediments is calculated for the granitic catchments in
719 southeastern Australia and Puerto Rico. Values for the Nunnock River range from 350 ± 10 kyr
720 to 1.8 ± 0.2 Myr and are greater than weathering ages calculated for the Rio Icacos/Sabana (5.1
721 ± 0.1 to 19.4 ± 0.4 kyr). The range in weathering ages inferred for both regions is interpreted as
722 reflecting the dominant mechanism for erosion operating in these catchments: near-surface soil
723 transport for the Nunnock River, mobilizing sediments from the top of old weathering profiles
724 (in this case the weathering age also reflects the time required to develop these profiles) and
725 landslides for Puerto Rico, where sediments originate from deeper parts of the weathering
726 profile.

727 Using the model of Yoo and Mudd (2008), weathering ages can be used to calculate
728 catchment-wide weathering rates. In Puerto Rico, we infer mineral-specific sediment
729 weathering rates that agree with previous independent estimates from soil profiles (Buss et al.,
730 2008; Ferrier et al., 2010; Murphy et al., 1998; Schulz and White, 1999). This demonstrates that,
731 if mineralogical parameters and average weathering profile thicknesses are known, U-series
732 weathering ages of stream sediments may be useful for estimating catchment-wide weathering
733 rates in small catchments. For the southeastern Australian catchment, calculated mineral
734 weathering rates are slower. Differences in weathering rates between southeastern Australia
735 and Puerto Rico are mostly accounted for by contrasting weathering ages, which in turn are
736 controlled by the dominant type of catchment erosion operating in each catchment (near-
737 surface soil transport vs. landslides). Where landslides dominate, minerals bypass at least part

of the weathering profile thus supplying the lower catchment with sediments rich in soluble mineral phases that can undergo further weathering. In contrast, where near-surface soil transport dominates, the regolith mobilised into the river has already undergone extensive weathering and little additional weathering is expected during sediment transport. Consequently, the type of erosion in the upper catchment determines the possibility for further weathering during sediment transport and storage in alluvial plains, recently postulated to dominate global weathering fluxes (Lupker et al., 2012).

Acknowledgements

Logistical support was partially contributed by the NSF-supported Luquillo Critical Zone Observatory (NSF-LCZO, grant EAR 0722476 to F. Scatena, Univ. of Pennsylvania). Joseph Troester is thanked for support in the field and helpful discussions, Manuel Rosario Torres and all the staff at the US Geological Survey (USGS) Guaynabo, Puerto Rico, for their help and facilitating sample processing after collection. We also thank Grant Douglas for help with filtration logistics and Derek Fabel for preparing soil quartz samples. AD is supported by an Australian Research Council Future Fellowship (FT0990447). HLB acknowledges support of the USGS Water Energy and Biogeochemical Budgets program. This work was supported by two Australian Research Council Discovery grants (DP0451704 and DP1093708).

References

Ames, L.L., McGarrah, J.E., Walker, B.A., 1983a. Sorption of trace constituents from aqueous solutions onto secondary minerals. II Radium. Clays Clay Miner. 31, 335-342.

Ames, L.L., McGarrah, J.E., Walker, B.A., 1983b. Sorption of uranium and radium by biotite, muscovite and phlogopite. Clays Clay Miner. 31, 343-351.

Andersen, M.B., Vance, D., Keech, A., Rickli, J., Hudson, G., 2013. Estimating U fluxes in a high-latitude, boreal post-glacial setting using U-series isotopes in soils and rivers. Chemical Geology.

Andersson, P.S., Wasserburg, G.J., Chen, J.H., Papanastassiou, D.A., 1995. ^{238}U-^{234}U and ^{232}Th-^{230}Th in the Baltic Sea and in river water. Earth Planet. Sci. Lett. 130, 217-234.

Bengtsson, L., Enell, M., 1986. Chemical analysis, in: Berglund, B.E. (Ed.), Handbook of Holocene Palaeoecology and Palaeohydrology. John Wiley & Sons Ldt., Chichester, pp. 423-451.

Borole, D.V., Krishnaswami, S., Somayajulu, B.L.K., 1982. Uranium isotopes in rivers, estuaries and adjacent coastal sediments of western India: their weathering, transport and oceanic budget. Geochimica et Cosmochimica Acta 46, 125-137.

Bouchez, J., Gaillardet, J., Lupker, M., Louvat, P., France-Lanord, C., Maurice, L., Armijos, E., Moquet, J.-S., 2012. Floodplains of large rivers: Weathering reactors or simple silos? Chemical Geology 332-333, 166-184.

Bouchez, J., Lupker, M., Gaillardet, J., France-Lanord, C., Maurice, L., 2011. How important is it to integrate riverine suspended sediment chemical composition with depth? Clues from Amazon River depth-profiles. Geochimica et Cosmochimica Acta 75, 6955-6970.

Braun, J., Heimsath, A.M., Chappell, J., 2001. Sediment transport mechanisms on soil-mantled hillslopes. Geology 29, 683-686.

Brown, E.T., Stallard, R.F., Larsen, M.C., Raisbeck, G.M., Yiou, F., 1995. Denudation rates determined from the accumulation of in-situ produced 10Be in the Luquillo Experimental Forest, Puerto Rico. Earth and Planetary Science Letters 129, 193-202.

Bureau of Meteorology Australia, 1999. Climate average for Bega, NSW, 1879-1996; Bombala, NSW, 1885-1996; and Nimmitabel, NSW, 1894-1996.

Burg, J.P., Wilson, C.J.L., 1988. A kinematic analysis of the southernmost part of the Bega Batholith. Australian Journal of Earth Sciences 35, 1-13.

Buss, H., White, A., 2012. Weathering Processes in the Rio Icacos Watershed, in: Murphy, S.F., Stallard, R.F. (Eds.), Water Quality and Landscape Processes of Four Watersheds in Eastern Puerto Rico, pp. 249-262.

Buss, H.L., Brantley, S.L., Scatena, F.N., Bazilievskaya, E.A., Blum, A., Schulz, M., Jimenez, R., White, A.F., Rother, G., Cole, D., 2013. Probing the deep critical zone beneath the Luquillo Experimental Forest, Puerto Rico. Earth Surf. Proc. Landforms 38, 1170-1186.

Buss, H.L., Bruns, M.A., Schultz, M.J., Moore, J., Mathur, C.F., Brantley, S.L., 2005. The coupling of biological iron cycling and mineral weathering during saprolite formation, Luquillo Mountains, Puerto Rico. Geobiology 3, 247-260.

Buss, H.L., Mathur, R., White, A.F., Brantley, S.L., 2010. Phosphorus and iron cycling in deep saprolite, Luquillo Mountains, Puerto Rico. Chemical Geology 269, 52-61.

Buss, H.L., Sak, P.B., Webb, S.M., Brantley, S.L., 2008. Weathering of the Rio Blanco quartz diorite, Luquillo Mountains, Puerto Rico: Coupling oxidation, dissolution, and fracturing. Geochimica et Cosmochimica Acta 72, 4488-4507.

Chabaux, F., Allègre, C.J., 1994. ^{238}U-^{230}Th-^{226}Ra disequilibria in volcanics: A new insight into melting conditions. Earth Planet. Sci. Lett. 126, 61-74.
Chabaux, F., Blaes, E., Stille, P., di Chiara Roupert, R., Pelt, E., Dosseto, A., Ma, L., Buss, H.L., Brantley, S.L., 2013. Regolith formation rate from U-series nuclides: Implications from the study of a spheroidal weathering profile in the Rio Icacos watershed (Puerto Rico). Geochimica et Cosmochimica Acta 100, 73-95.
Chabaux, F., Bourdon, B., Riotte, J., 2008. U-Series Geochemistry in Weathering Profiles, River Waters and Lakes, Radioactivity in the Environment. Elsevier.
Chabaux, F., Dequincey, O., Leveque, J.-J., Leprun, J.-C., Clauer, N., Riotte, J., Paquet, H., 2003a. Tracing and dating recent chemical transfers in weathering profiles by trace-element geochemistry and 238U---234U---230Th disequilibria: the example of the Kaya lateritic toposequence (Burkina-Faso). Comptes Rendus Geosciences 335, 1219-1231.
Chabaux, F., Granet, M., Pelt, E., France-Lanord, C., Galy, V., 2006. ^{238}U-^{234}U-^{230}Th disequilibria and timescale of sedimentary transfers in rivers: Clues from the Gangetic plain rivers. Journal of Geochemical Exploration 88, 373-375.
Chabaux, F., Riotte, J., Dequincey, O., 2003b. U-Th-Ra fractionation during weathering and river transport, in: Bourdon, B., Henderson, G.M., Lundstrom, C.C., Turner, S.P. (Eds.), Uranium-series Geochemistry. Geochemical Society - Mineralogical Society of America, Washington, pp. 533-576.
Chamberlain, C.P., Waldbauer, J.R., Jacobson, A.D., 2005. Strontium, hydrothermal systems and steady-state chemical weathering in active mountain belts. Earth and Planetary Science Letters 238, 351-366.
Cheng, H., Lawrence Edwards, R., Shen, C.-C., Polyak, V.J., Asmerom, Y., Woodhead, J., Hellstrom, J., Wang, Y., Kong, X., Spötl, C., Wang, X., Calvin Alexander Jr, E., 2013. Improvements in 230Th dating, 230Th and 234U half-life values, and U–Th isotopic measurements by multi-collector inductively coupled plasma mass spectrometry. Earth and Planetary Science Letters 371–372, 82-91.
Dean, W.E., 1974. Determination of carbonate and organic matter in calcareous sediments and sedimentary rocks by loss on ignition; comparison with other methods. Journal of sedimentary research 44, 242-248.
DePaolo, D.J., Maher, K., Christensen, J.N., McManus, J., 2006. Sediment transport time measured with U-series isotopes: Results from ODP North Atlantic drift site 984. Earth and Planetary Science Letters 248, 394-410.
Dequincey, O., Chabaux, F., Clauer, N., Liewig, N., Muller, J.-P., 1999. Dating of weathering profiles by radioactive disequilibria: Contribution of the study of authigenic mineral fractions. Comptes Rendus de l'Academie des Sciences - Series IIA - Earth and Planetary Science 328, 679-685.
Dequincey, O., Chabaux, F., Clauer, N., Sigmarsson, O., Liewig, N., Leprun, J.-C., 2002. Chemical mobilizations in laterites: Evidence from trace elements and ^{238}U-^{234}U-^{230}Th disequilibria. Geochim. Cosmochim. Acta 66, 1197-1210.
Dixon, J.L., Heimsath, A.M., Amundson, R., 2009. The critical role of climate and saprolite weathering in landscape evolution. Earth Surface Processes and Landforms 34, 1507-1521.
Donkin, M.J., 1991. Loss-on-ignition as an estimator of soil organic carbon in A-horizon forestry soils. Communications in Soil Science & Plant Analysis 22, 233-241.

Dosseto, A., Bourdon, B., Gaillardet, J., Allègre, C.J., Filizola, N., 2006a. Timescale and conditions of chemical weathering under tropical climate: Study of the Amazon basin with U-series. Geochim. Cosmochim. Acta 70, 71-89.

Dosseto, A., Bourdon, B., Gaillardet, J., Maurice-Bourgoin, L., Allègre, C.J., 2006b. Weathering and transport of sediments in the Bolivian Andes: time constraints from uranium-series isotopes. Earth and Planetary Science Letters 248, 759-771.

Dosseto, A., Bourdon, B., Turner, S.P., 2008a. Uranium-series isotopes in river materials: Insights into the timescales of erosion and sediment transport. Earth and Planetary Science Letters 265, 1-17.

Dosseto, A., Buss, H., Suresh, P.O., 2011. The delicate balance between soil production and erosion, and its role on landscape evolution. Applied Geochemistry 26, S24-S27.

Dosseto, A., Buss, H.L., Suresh, P.O., 2012. Rapid regolith formation over volcanic bedrock and implications for landscape evolution. Earth and Planetary Science Letters 337–338, 47-55.

Dosseto, A., Hesse, P., Maher, K., Fryirs, K., Turner, S.P., 2010. Climatic and vegetation control on sediment dynamics. Geology 38, 395-398.

Dosseto, A., Turner, S., Buss, H.L., Chabaux, F., 2007. The timescale of sediment transport in a small tropical watershed. Geochim. Cosmochim. Acta 71, Suppl. 1.

Dosseto, A., Turner, S., Douglas, G.B., 2006c. Uranium-series isotopes in colloids and suspended sediments: timescale for sediment production and transport in the Murray-Darling River system. Earth Planet. Sci. Lett. 246, 418-431.

Dosseto, A., Turner, S.P., Chappell, J., 2008b. The evolution of weathering profiles through time: New insights from uranium-series isotopes. Earth and Planetary Science Letters 274, 359-371.

Douglas, G.B., 1993. Characterization of suspended particulate matter in the Murray-Darling River system. Monash University, Melbourn.

Eggins, S.M., Woodhead, J.D., Kinsley, L.P.J., Mortimer, G.E., Sylvester, P., McCulloch, M.T., Hergt, J.M., Handler, M.R., 1997. A simple method for the precise determination of ≥ 40 trace elements in geological samples by ICPMS using enriched isotope internal standardisation. Chemical Geology 134, 311-326.

Ferrier, K.L., Kirchner, J.W., 2008. Effects of physical erosion on chemical denudation rates: A numerical modeling study of soil-mantled hillslopes. Earth and Planetary Science Letters 272, 591-599.

Ferrier, K.L., Kirchner, J.W., Riebe, C.S., Finkel, R.C., 2010. Mineral-specific chemical weathering rates over millennial timescales: Measurements at Rio Icacos, Puerto Rico. Chemical Geology 277, 101-114.

Fleischer, R.L., 1980. Isotopic disequilibrium of uranium: Alpha-recoil damage and preferential solution effects. Science 207, 979-981.

Fleischer, R.L., 1982a. Alpha-recoil damage and solution effects in minerals: uranium isotopic disequilibrium and radon release. Geochimica et Cosmochimica Acta 46, 2191-2201.

Fleischer, R.L., 1982b. Nature of alpha-recoil damage: Evidence from preferential solution effects. Nuclear Tracks and Radiation Measurements (1982) 6, 35-42.

Fleischer, R.L., Raabe, O.G., 1978. Recoiling alpha-emitting nuclei. Mechanisms for uranium-series disequilibrium. Geochimica et Cosmochimica Acta 42, 973-978.

Gaillardet, J., Dupré, B., Allègre, C.J., 1995. A global mass budget applied to the Congo Basin rivers: Erosion rates and continental crust composition. Geochim. Cosmochim. Acta 59, 3469-3485.

Gaillardet, J., Dupré, B., Allègre, C.J., Négrel, P., 1997. Chemical and physical denudation in the Amazon River Basin. Chem. Geol. 142, 141-173.

Goldin, A., 1987. Reassessing the use of loss-on-ignition for estimating organic matter content in noncalcareous soils. Communications in Soil Science & Plant Analysis 18, 1111-1116.

Granet, M., Chabaux, F., Stille, P., Dosseto, A., France-Lanord, C., Blaes, E., 2010. U-series disequilibria in suspended river sediments and implication for sediment transfer time in alluvial plains: The case of the Himalayan rivers. Geochim. Cosmochim. Acta 74, 2851-2865.

Granet, M., Chabaux, F., Stille, P., France-Lanord, C., Pelt, E., 2007. Time-scales of sedimentary transfer and weathering processes from U-series nuclides: Clues from the Himalayan rivers. Earth and Planetary Science Letters 261, 389-406.

Green, E.G., Dietrich, W.E., Banfield, J.F., 2006. Quantification of chemical weathering rates across an actively eroding hillslope. Earth Planet. Sci. Lett. 242, 155-169.

Grzymko, T.J., Marcantonio, F., McKee, B.A., Mike Stewart, C., 2007. Temporal variability of uranium concentrations and 234U/238U activity ratios in the Mississippi river and its tributaries. Chemical Geology 243, 344-356.

Heartsill-Scaley, T., Scatena, F.N., Estrada, C., McDowell, W.H., Lugo, A.E., 2007. Disturbance and long-term patterns of rainfall and throughfall nutrient fluxes in a subtropical wet forest in Puerto Rico. Journal of Hydrology 333, 472-485.

Heimsath, A.M., Chappell, J., Dietrich, W.E., Nishiizumi, K., Finkel, R.C., 2000. Soil production on a retreating escarpment in southeastern Australia. Geology 28, 787-790.

Heimsath, A.M., Chappell, J., Spooner, N.A., Questiaux, D.G., 2002. Creeping soil. Geology 30, 111-114.

Heiri, O., Lotter, A.F., Lemcke, G., 2001. Loss on ignition as a method for estimating organic and carbonate content in sediments: reproducibility and comparability of results. Journal of Paleolimnology 25, 101-110.

Hidaka, H., Horie, K., Gauthier-Lafaye, F., 2007. Transport and selective uptake of radium into natural clay minerals. Earth and Planetary Science Letters 264, 167-176.

Hussain, N., Lal, D., 1986. Preferential solution of ^{234}U from recoil tracks and $^{234}U/^{238}U$ radioactive disequilibrium in natural waters. Proceedings of the Indian Academy of Sciences - Earth and Planetary Sciences 95, 245-263.

Jolly, W.T., Lidiak, E.G., Dickin, A.P., Wu, T.-W., 1998a. Geochemical diversity of Mesozoic island arc tectonic blocks in eastern Puerto Rico, in: Lidiak, E.G., Larue, D.K. (Eds.), Tectonics and geochemistry of the northeastern Caribbean. Geological Society of America, Boulder, Colorado, pp. 67-98.

Jolly, W.T., Lidiak, E.G., Schellenkens, J.H., Santos, J., 1998b. Volcanism, tectonic and stratigraphic correlations in Puerto Rico, in: Lidiak, E.G., Larue, D.K. (Eds.), Tectonics and geochemistry of the northeastern Caribbean. Geological Society of America, Boulder, Colorado, pp. 1-34.

Keech, A.R., West, A.J., Pett-Ridge, J.C., Henderson, G.M., 2013. Evaluating U-series tools for weathering rate and duration on a soil sequence of known ages. Earth and Planetary Science Letters.

929 Kigoshi, K., 1971. Alpha-recoil thorium-234: Dissolution into water and the uranium-
930 234/uranium-238 disequilibrium in nature. Science 173, 47-48.
931 Kohl, C.P., Nishiizumi, K., 1992. Chemical isolation of quartz for measurement of in-situ -
932 produced cosmogenic nuclides. Geochimica et Cosmochimica Acta 56, 3583-3587.
933 Kraemer, T.F., Brabets, T.P., 2012. Uranium isotopes (234U/238U) in rivers of the Yukon Basin
934 (Alaska and Canada) as an aid in identifying water sources, with implications for monitoring
935 hydrologic change in arctic regions. Hydrogeology Journal 20, 469-481.
936 Krishnaswami, S., Williams, G.A., Graustein, W.C., Turekian, K.K., 2004. The effect of weathering
937 regime on uranium decay series and osmium in two soil profiles. Geochemical Journal 38, 651-
938 660.
939 Kurtz, A.C., Lugolobi, F., Salvucci, G., 2011. Germanium-silicon as a flow path tracer: Application
940 to the Rio Icacos watershed. Water Resources Research 47.
941 Larsen, M.C., 2012. Landslides and Sediment Budgets in Four Watersheds in Eastern Puerto
942 Rico, in: Murphy, S.F., Stallard, R.F. (Eds.), Water Quality and Landscape Processes of Four
943 Watersheds in Eastern Puerto Rico, p. 292.
944 Larsen, M.C., Stallard, R.F., 2000. Luquillo Mountains, Puerto Rico. A water, energy, and
945 biogeochemical budgets program site. USGS Fact Sheet 163-99.
946 Larsen, M.C., Torres-Sánchez, A.J., 1992. Landslides Triggered by Hurricane Hugo in Eastern
947 Puerto Rico, September 1989. Caribbean Journal of Science 28, 113-125.
948 Lee, V., DePaolo, D.J., Christensen, J.N., 2010. Uranium-series comminution ages of continental
949 sediments: Case study of a Pleistocene alluvial fan. Earth and Planetary Science Letters 296,
950 244-254.
951 Lupker, M., France-Lanord, C., Galy, V., Lavé, J., Gaillardet, J., Gajurel, A.P., Guilmette, C.,
952 Rahman, M., Singh, S.K., Sinha, R., 2012. Predominant floodplain over mountain weathering of
953 Himalayan sediments (Ganga basin). Geochimica et Cosmochimica Acta 84, 410-432.
954 Ma, L., Chabaux, F., Pelt, E., Blaes, E., Jin, L., Brantley, S.L., 2010. Regolith production rates
955 calculated with uranium-series isotopes at Susquehanna/Shale Hills Critical Zone Observatory.
956 Earth and Planetary Science Letters 297, 211-255.
957 Marx, S.K., Kamber, B.S., McGowan, H.A., 2005. Estimates of Australian dust flux into New
958 Zealand: Quantifying the eastern Australian dust plume pathway using trace element calibrated
959 210Pb as a monitor. Earth and Planetary Science Letters 239, 336-351.
960 Murphy, S.F., Brantley, S.L., Blum, A.E., White, A.F., Dong, H., 1998. Chemical weathering in a
961 tropical watershed, Luquillo Mountains, Puerto Rico: II. Rate and mechanism of biotite
962 weathering. Geochimica et Cosmochimica Acta 62, 227-243.
963 Ollier, C.D., 1982. The great escarpement of Eastern Australia: tectonic and geomorphic
964 significance. J. Geol. Soc. Aust. 29, 13-23.
965 Pelt, E., Chabaux, F., Innocent, C., Navarre-Sitchler, A.K., Sak, P.B., Brantley, S.L., 2008. Uranium-
966 thorium chronometry of weathering rinds: Rock alteration rate and paleo-isotopic record of
967 weathering fluids. Earth and Planetary Science Letters 276, 98-105.
968 Peters, N.E., Shanley, J.B., Aulenbach, B.T., Webb, R.M., Campbell, D.H., Hunt, R., Larsen, M.C.,
969 Stallard, R.F., Troester, J., Walker, J.F., 2006. Water and solute mass balance of five small,
970 relatively undisturbed watersheds in the U.S. Science of The Total Environment 358, 221-242.

971 Pett-Ridge, J.C., Derry, L.A., Barrows, J.K., 2009a. Ca/Sr and 87Sr/86Sr ratios as tracers of Ca and
972 Sr cycling in the Rio Icacos watershed, Luquillo Mountains, Puerto Rico. Chemical Geology 267,
973 32-45.
974 Pett-Ridge, J.C., Derry, L.A., Kurtz, A.C., 2009b. Sr isotopes as a tracer of weathering processes
975 and dust inputs in a tropical granitoid watershed, Luquillo Mountains, Puerto Rico. Geochimica
976 et Cosmochimica Acta 73, 25-43.
977 Pietruszka, A.J., Carlson, R.W., Hauri, E.H., 2002. Precise and accurate measurement of 226Ra-
978 230Th-238U disequilibria in volcanic rocks using plasma ionization multicollector mass
979 spectrometry. Chem. Geol. 188, 171-191.
980 Plater, A.J., Ivanovich, M., Dugdale, R.E., 1992. Uranium series disequilibrium in river sediments
981 and waters: The significance of anomalous activity ratios. Appl. Geochem. 7.
982 Pogge von Strandmann, P.A.E., Burton, K.W., Porcelli, D., James, R.H., van Calsteren, P.,
983 Gislason, S.R., 2011. Transport and exchange of U-series nuclides between suspended material,
984 dissolved load and colloids in rivers draining basaltic terrains. Earth and Planetary Science
985 Letters 301, 125-136.
986 Porcelli, D., Andersson, P.S., Baskaran, M., Wasserburg, G.J., 2001. Transport of U- and Th-series
987 nuclides in a Baltic Shield watershed and the Baltic Sea. Geochim. Cosmochim. Acta 65, 2439-
988 2459.
989 Price, R.C., George, R., Gamble, J.A., Turner, S., Smith, I.E.M., Cook, C., Hobden, B., Dosseto, A.,
990 2007. U-Th-Ra fractionation during crustal-level andesite formation at Ruapehu volcano, New
991 Zealand. Chemical Geology 244, 437-451.
992 Prosser, I., Moran, C.J., Lu, H., Olley, J., DeRose, R., Cannon, G., Croke, B., Hughes, A., Jakeman,
993 T., Newham, L., Scott, A., Weisse, M., 2003. Basin-wide mapping of sediment and nutrient
994 exports in dryland regions of the Murray-Darling basin. CSIRO Land and Water, Canberra, pp. 1-
995 38.
996 Prosser, I.P., Rutherfurd, I.D., Olley, J.M., Young, W.J., Wallbrink, P.J., Moran, C.J., 2001. Large-
997 scale patterns of erosion and sediment transport in river networks, with examples from
998 Australia. Marine and Freshwater Research 52, 81-99.
999 Riebe, C.S., Kirchner, J.W., Finkel, R.C., 2003. Long-term rates of chemical weathering and
1000 physical erosion from cosmogenic nuclides and geochemical mass balance. Geochim.
1001 Cosmochim. Acta 67, 4411-4427.
1002 Riotte, J., Chabaux, F., 1999. ($^{234}U/^{238}U$) activity ratios in freshwaters as tracers of hydrological
1003 processes: the Strengbach watershed (Vosges, France). Geochim. Cosmochim. Acta 63, 1263-
1004 1275.
1005 Sarin, M.M., Krishnaswami, S., Somayajulu, B.L.K., Moore, W.S., 1990. Chemistry of uranium,
1006 thorium, and radium isotopes in the Ganga-Brahmaputra river system: Weathering processes
1007 and fluxes to the Bay of Bengal. Geochim. Cosmochim. Acta 54, 1387-1396.
1008 Schulz, M.S., White, A.F., 1999. Chemical weathering in a tropical watershed, Luquillo
1009 Mountains, Puerto Rico III: Quartz dissolution rates. Geochimica et Cosmochimica Acta 63, 337-
1010 350.
1011 Sims, K.W.W., Gill, J.B., Dosseto, A., Hoffmann, D.L., Lundstrom, C.C., Williams, R.W., Ball, L.,
1012 Tollstrup, D., Turner, S., Prytulak, J., Glessner, J.J.G., Standish, J.J., Elliott, T., 2008. An Inter-
1013 Laboratory Assessment of the Thorium Isotopic Composition of Synthetic and Rock Reference
1014 Materials. Geostandards and Geoanalytical Research 32, 65-91.

Smith, A.L., Schellenkens, J.H., Diaz, A.M., 1998. Batholiths as markers of tectonic change in the northeastern Caribbean, in: Lidiak, E.G., Larue, D.K. (Eds.), Tectonics and Geochemistry of the Northeastern Caribbean. Geologic Society of America, Boulder, Colorado, pp. 99-122.
Spain, A.V., Probert, M.E., Isbell, R.F., John, R.D., 1982. Loss-on-ignition and the carbon contents of Australian soils. Australian Journal of Soil Research 20, 147-152.
Turner, B.F., Stallard, R.F., Brantley, S.L., 2003. Investigation of in situ weathering of quartz diorite bedrock in the Rio Icacos basin, Luquillo Experimental Forest, Puerto Rico. Chemical Geology 202, 313-341.
Turner, S., Bourdon, B., Hawkesworth, C., Evans, P., 2000. ^{226}Ra-^{230}Th evidence for multiple dehydration events, rapid melt ascent and time scales of differentiation beneath the Tonga-Kermadec island arc. Earth Planet. Sci. Lett. 179, 581-593.
Vigier, N., Bourdon, B., 2011. Constraining Rates of Chemical and Physical Erosion Using U-Series Radionuclides, in: Baskaran, M. (Ed.), Handbook of Environmental Isotope Geochemistry. Springer Berlin Heidelberg, pp. 553-571.
Vigier, N., Bourdon, B., Lewin, É., Dupré, B., Turner, S., Van Calsteren, P., Subramanian, V., Allègre, C.J., 2005. Mobility of U-series nuclides during basalt weathering: An example of the Deccan Traps (India). Chem. Geol. 219, 69-91.
Vigier, N., Bourdon, B., Turner, S., Allègre, C.J., 2001. Erosion timescales derived from U-decay series measurements in rivers. Earth Planet. Sci. Lett. 193, 546-563.
Vigier, N., Burton, K.W., Gislason, S.R., Rogers, N.W., Duchene, S., Thomas, L., Hodge, E., Schaefer, B., 2006. The relationship between riverine U-series disequilibria and erosion rates in a basaltic terrain. Earth and Planetary Science Letters 249, 258-273.
White, A.F., Blum, A.E., Schulz, M.S., Bullen, T.D., Harden, J.W., Peterson, M.L., 1996. Chemical weathering rates of a soil chronosequence on granitic alluvium: I. Quantification of mineralogical and surface area changes and calculation of primary silicate reaction rates. Geochimica et Cosmochimica Acta 60, 2533-2550.
White, A.F., Blum, A.E., Schulz, M.S., Vivit, D.V., Stonestrom, D.A., Larsen, M., Murphy, S.F., Eberl, D., 1998. Chemical weathering in a tropical watershed, Luquillo Mountains, Puerto Rico: I. Long-term versus short-term weathering fluxes. Geochim. Cosmochim. Acta 62, 209-226.
White, A.F., Brantley, S.L., 2003. The effect of time on the weathering of silicate minerals: why do weathering rates differ in the laboratory and field? Chemical Geology 202, 479-506.
White, A.J.R., Chappell, B.W., 1983. Granitoid types and their distribution in the Lachlan Fold Belt, southeastern Australia, in: Roddick, J.A. (Ed.), Circum-Pacific Plutonic Terranes. Geological Society of America, pp. 21-34.
Yoo, K., Mudd, S.M., 2008. Discrepancy between mineral residence time and soil age: Implications for the interpretation of chemical weathering rates. Geology 36, 35-38.

Figure captions

Figure 1. Illustration of the concept of *sediment weathering age* in the case where transport time of sediments in the river is short compared to the storage time in weathering profiles. (a) In a weathering profile, the weathering front is postulated to progress downward. At time t = T_1, the weathering front is at the elevation of regolith sample R_1 (assuming no uplift); at t = T_2, the weathering front is at the elevation of regolith sample R_7. At t = T_3, the weathering age of regolith samples R1 and R7 is $T_{w,R1} = T_3 - T_1$ and $T_{w,R7} = T_3 - T_2$, respectively. (b) Assuming that erosion occurs shortly after T_3 (t = $T_3 + \varepsilon$), if near-surface soil transport is dominant and only the top of the profile is eroded, the weathering age of sediments, $T_{w,S1}$, is similar to that of the regolith at the top of the weathering profile, $T_{w,R1}$. (c) However, if landslides dominate, the sediment weathering age, $T_{w,S2}$, will be younger than $T_{w,S1}$ since it will include regolith with a younger age (e.g. $T_{w,R7}$) and integrates regolith ages over the depth of the landslide. (d) Representation of the possible U-series isotope composition of regolith R1 and R7, and sediments S1 and S2.

Figure 2. (a) Location map of stream samples (dots) in the Nunnock River basin, southeastern Australia. The location of the weathering profiles studied in Dosseto et al. (2008b) is also shown (square). (b) Location map of stream samples (dots) in Rio Icacos, Sabana and Mameyes basins, in the Luquillo Mountains, eastern Puerto Rico. The location of the LG1 weathering profile studied in (Dosseto et al., 2007; White et al., 1998) and the Bisley weathering profile studied in (Dosseto et al., 2011; Dosseto et al., 2012) are also shown (squares). The inset shows Puerto Rico and the Luquillo Mountains in the Greater Antilles. The topographic maps are taken from Google Maps™.

Figure 3. U (squares; in ppm), Th (diamonds; in ppm) and ^{226}Ra (triangles; in fg/g) concentrations as a function of the Loss on Ignition (LOI; in wt. %) in suspended sediments from the Nunnock River catchment. This illustrates how organic matter, metal oxides and clays control the budget of these nuclides in the river suspended load. If not shown, error bars are smaller than the symbol size.

Figure 4. U-series isotope composition in river-borne material from the Nunnock River, southeastern Australia. (a) ($^{234}U/^{238}U$) and (b) ($^{226}Ra/^{230}Th$) versus ($^{230}Th/^{238}U$) activity ratios. (c) ($^{230}Th/^{232}Th$) versus ($^{238}U/^{232}Th$) activity ratios. Equilines (i.e. secular equilibrium) are shown as dashed lines. In (c), the composition of saprolite, soil and bedrock from the same catchment are taken from Dosseto et al. (2008b).

Figure 5. U-Th geochemical variations across size fractions for Puerto Rico streams: (a) U and (b) Th concentrations (in ppm), (c) ($^{234}U/^{238}U$), (d) ($^{230}Th/^{234}U$), (e) ($^{230}Th/^{232}Th$) activity ratios and (e) U/Th ratio. Thick lines are the compositions of size fractions from tangential filtration, while thin lines are the compositions of the <0.2 μm fraction obtained by "frontal filtration" at 0.2 μm (see Analytical Techniques).

Figure 6. Evolution curves for different sets of parameters of the nuclide gain/loss model. For the three upper curves: w_{238} = 10^{-5} yr^{-1}, Γ_{238}/w_{238} = 0.1, w_{234}/w_{238}= 1.05, w_{230}/w_{238} = 0.5, $\Gamma_{230}/\Gamma_{238}$ = 0.2 and the bold italicised numbers on the curves are $\Gamma_{234}/\Gamma_{238}$ values (1.1, 1.15 and 1.2). For the three lower curves: w_{238} = $2x10^{-5}$ yr^{-1}, $\Gamma_{234}/\Gamma_{238}$ = 0.9, w_{234}/w_{238}= 1.05, w_{230}/w_{238} = 0.1, $\Gamma_{230}/\Gamma_{238}$ = 10^{-10} and the bold italicised numbers on the curves are Γ_{238}/w_{238} values (0.2, 0.5 and 1). Tick marks are modelled weathering ages. Symbols are data from the Nunnock River (squares: suspended sediments; diamonds: bedload sediments). Note that because data do not describe a well-defined trend, ages cannot be simply read off evolution curves. Instead, the best set of parameters is defined by the median of the large population of solutions (n > 1000) generated by inversion of the ($^{234}U/^{238}U$) and ($^{230}Th/^{238}U$) activity ratios.

Figure A1. Variations in ($^{230}Th/^{232}Th$) activity ratios versus depth for regolith samples of the LG1 weathering profile (see Fig. 2 for location). Despite unusual large errors possibly reflecting sample heterogeneity, there is a statistically significant increase in ($^{230}Th/^{232}Th$) between the saprock, saprolite and soil (Table A2).

Table 1

Table 1. U-series composition of Nunnock River samples

Size fractions <0.2 μm (dissolved+colloidal load)

Sample ID	Th (ng/L)	U (ng/L)	^{226}Ra (fg/L)	(^{234}U/^{238}U)	Std.Err.	(^{230}Th/^{238}U)	Std.Err.	(^{226}Ra/^{230}Th)	Std.Err.	(^{238}U/^{232}Th)	Std.Err.	(^{230}Th/^{232}Th)	Std.Err.
NUN01		29.1	29.5	1.058	0.004								
NUN02	245.2	61.2	22.0	1.082	0.003	0.610	0.002	1.720	0.014	0.758	0.001	0.462	0.002
NUN03	187.5	57.7	24.6	1.056	0.004	0.499	0.002	2.495	0.016	0.934	0.001	0.466	0.002
NUN04	211.0	62.4	27.1	1.144	0.003	0.510	0.002	2.487	0.019	0.897	0.001	0.457	0.002
NUN05	229.4	84.2	27.93	1.167	0.003	0.412	0.002	2.351	0.021	1.114	0.001	0.459	0.002

Size fractions >0.2 μm (suspended load)

Sample ID	Th (ppm)	U (ppm)	^{226}Ra (fg/g)	(^{234}U/^{238}U)	Std.Err.	(^{230}Th/^{238}U)	Std.Err.	(^{226}Ra/^{230}Th)	Std.Err.	(^{238}U/^{232}Th)	Std.Err.	(^{230}Th/^{232}Th)	Std.Err.	LOI (wt. %)	Suspended matter concentration (mg/L)
NUN01	30.4	6.26	2508	1.049	0.003	1.004	0.007	1.155	0.004	0.626	0.002	0.628	0.004	0.49	12.4
NUN02	24.7	5.31	3142	1.005	0.004	0.891	0.006	1.923	0.005	0.652	0.002	0.581	0.003	0.53	5.8
NUN03	16.8	4.61	2057	1.042	0.005	0.967	0.006	1.320	0.006	0.830	0.002	0.803	0.004	0.24	2.3
NUN04	35.5	8.30	3304	1.066	0.003	0.866	0.004	1.315	0.005	0.710	0.002	0.615	0.002	0.71	7.5
NUN05	35.0	8.49	3186	1.079	0.003	0.827	0.003	1.298	0.003	0.736	0.002	0.608	0.001	0.55	9.6

Bedload sediments

Sample ID	Th (ppm)	U (ppm)	^{226}Ra (fg/g)	(^{234}U/^{238}U)	Std.Err.	(^{230}Th/^{238}U)	Std.Err.	(^{226}Ra/^{230}Th)	Std.Err.	(^{238}U/^{232}Th)	Std.Err.	(^{230}Th/^{232}Th)	Std.Err.	LOI (wt. %)
NUN03	3.54	0.672	291	0.894	0.001	0.993	0.004	1.278	0.005	0.576	0.001	0.572	0.002	1.22
NUN04	3.71	0.830	314	0.856	0.001	1.006	0.004	1.102	0.032	0.679	0.001	0.683	0.002	1.03
NUN05	2.99	0.721	269	0.858	0.001	1.045	0.004	1.046	0.018	0.732	0.001	0.765	0.003	0.78

Soil quartz separates

Sample ID	Th (ppm)	U (ppm)		(^{234}U/^{238}U)	Std.Err.	(^{230}Th/^{238}U)	Std.Err.			(^{238}U/^{232}Th)	Std.Err.	(^{230}Th/^{232}Th)	Std.Err.
Depth=30cm	0.085	0.012		0.980	0.002	2.72	0.01			0.414	0.001	1.125	0.005
Depth=50cm	0.075	0.019		0.976	0.007	2.02	0.02			0.768	0.005	1.553	0.006

Rock standard	Th (ppm)	U (ppm)	^{226}Ra (fg/g)	(^{234}U/^{238}U)	Std.Err.	(^{230}Th/^{238}U)	Std.Err.	(^{226}Ra/^{230}Th)	Std.Err.	(^{238}U/^{232}Th)	Std.Err.	(^{230}Th/^{232}Th)	Std.Err.
TML-3 (n=1)	29.79	10.58	3550	1.006	0.002	0.997	0.004	0.996	0.004	1.078	0.003	1.075	0.003

Reported errors are internal analytical uncertainties (2 standard errors). Relative 2σ errors on Th, U and ^{226}Ra concentrations are 6, 3 and 1%, respectively, and determined by replicate analysis of two solid sample aliquots.

Table 2

Table 2. Geochemical data for river material and rocks from Puerto Rico

Sample ID	River name	Size fraction	Th (ng/L)	U (ng/L)	(^{234}U/^{238}U)	Std.Err.	(^{230}Th/^{238}U)	Std.Err.	(^{238}U/^{232}Th)	Std.Err.	(^{230}Th/^{232}Th)	Std.Err.
RI-1	no name	<0.2µm	1.94	1.39					2.18	0.01		
RI-3	Mameyes	<0.2µm	1.34	2.73	1.14	0.01			6.19	0.24		
RI-3	Mameyes	<10kDa	0.95	2.62	1.193	0.008	0.197	0.008	8.36	0.13	1.64	0.08
RI-5	Sabana	<0.2µm	5.69	2.64	1.00	0.01			1.40	0.01		
RI-6	Icacos	<0.2µm	7.23	4.30					1.80	0.01		
RI-6	Icacos	<10kDa	2.01	1.90	1.062	0.009	0.344	0.014	2.87	0.01	0.99	0.04

Sample ID	River name	Size fraction	Th (ppm)	U (ppm)	^{226}Ra (fg/g)	Zr (ppm)	(^{234}U/^{238}U)	Std.Err.	(^{230}Th/^{238}U)	Std.Err.	(^{226}Ra/^{230}Th)	Std.Err.	(^{238}U/^{232}Th)	Std.Err.	(^{230}Th/^{232}Th)	Std.Err.	^{87}Sr/^{86}Sr	Std.Err.
RI-1	no name	>25µm	0.949	0.541	194.9	12.68	1.008	0.002	0.956	0.005	1.102	0.046	1.728	0.002	1.652	0.007	0.705020	0.000015
replicate			1.010	0.560	192.4		1.007	0.001	0.955	0.002	1.052	0.003	1.681	0.001	1.605	0.002		
RI-2	no name	bed sediments	0.898	0.572	170.6	7.9	0.998	0.001	0.882	0.002	0.897	0.003	1.934	0.002	1.707	0.003	0.705424	0.000022
RI-3	Mameyes	10-100kDa	0.789	1.156			1.126	0.002	0.434	0.001			4.442	0.003	1.928	0.004		
RI-3	Mameyes	100kDa-0.2µm	1.666	1.154			1.122	0.004	0.701	0.002			2.101	0.002	1.473	0.004		
RI-3	Mameyes	0.2-25µm	2.171	1.273			1.025	0.002	1.026	0.003			1.779	0.002	1.825	0.004		
RI-3	Mameyes	>25µm	0.386	0.328			0.792	0.001	0.812	0.002			2.577	0.002	2.091	0.006		
RI-3	Mameyes	bed sediments	1.716	1.574		54	0.773	0.002	0.815	0.002			2.782	0.004	2.266	0.003	0.705098	0.000012
RI-4	no name	bed sediments	0.567	0.239	95.7	6.0	0.996	0.004	1.155	0.006	1.012	0.004	1.278	0.001	1.477	0.003	0.704247	0.000020
RI-5	Sabana	10-100kDa	0.903	0.744			1.026	0.001	0.474	0.002			2.498	0.002	1.185	0.004		
RI-5	Sabana	100kDa-0.2µm	1.331	0.782			1.028	0.003	0.631	0.002			1.782	0.001	1.124	0.004		
RI-5	Sabana	0.2-25µm	3.067	1.282			1.008	0.001	0.992	0.004			1.268	0.001	1.258	0.004		
RI-5	Sabana	>25µm	2.247	1.137			1.009	0.002	0.854	0.003			1.536	0.001	1.311	0.003		
RI-5	Sabana	bed sediments	0.726	0.434	164.8	4.3	0.996	0.001	1.024	0.003	1.016	0.005	1.814	0.002	1.857	0.004	0.703942	0.000014
RI-6	Icacos	10-100kDa	0.607	0.420			1.038	0.002	0.563	0.002			2.099	0.002	1.181	0.004		
RI-6	Icacos	100kDa-0.2µm	3.389	1.419			1.033	0.002	0.872	0.002			1.270	0.001	1.108	0.002		
RI-6	Icacos	0.2-25µm	2.649	1.184			1.016	0.002	1.024	0.001			1.356	0.001	1.388	0.000		
RI-6	Icacos	>25µm	1.320	0.748	240.2	15.5	1.013	0.002	0.921	0.002	1.018	0.017	1.720	0.002	1.584	0.002	0.705612	0.000008
RI-6	Icacos	bed sediments	0.481	0.273	105.7	5.2	1.001	0.001	1.010	0.002	1.122	0.003	1.720	0.001	1.737	0.002	0.704550	0.000022
RI-7	Quebrada Guaba	>25µm	1.324	0.939	345.1	12.0	1.009	0.006	0.985	0.005	1.090	0.012	2.152	0.005	2.120	0.003	0.704715	0.000015
RI-7	Quebrada Guaba	bed sediments	0.810	0.366	125.6	8.3	0.989	0.004	1.038	0.006	0.968	0.005	1.369	0.001	1.420	0.004	0.704718	0.000020
RI-7	Quebrada Guaba	bank sediments	0.789	0.405		6.3	1.002	0.001	1.022	0.003			1.557	0.002	1.592	0.003	0.704717	0.000013
parent rock Icacos	n/a	n/a	0.348	0.241			1.002	0.002	1.140	0.003			2.099	0.002	2.392	0.005	0.70433	0.00016
parent rock Mameyes	n/a	n/a	1.044	0.747			0.993	0.002	0.808	0.003			2.170	0.003	1.754	0.005		

Reported errors are internal analytical uncertainties (2 standard errors), except for the ^{87}Sr/^{86}Sr where it is the standard deviation of 4 duplicate dissolutions of bedrock sample. Relative 2σ errors on Th, U and ^{226}Ra concentrations are 6, 3 and 1%, respectively, and determined by replicate analysis of two solid sample aliquots.

Table 3

Table 3. Solutions of the continuous loss-input nuclide model for Rio Icacos/Sabana catchments

w_{230}/w_{234} *set to* 10^{-10}					
Sample ID	T_{res} (kyr)	2std.err.		value	2std.err.
RI-4	174	3	w_{238} (yr^{-1})	4.65E-06	1.7E-07
Icacos	5.1	0.1	w_{234}/w_{238}	1.095	0.002
Quebrada Guaba bed	19.4	0.4	Γ_{238}/w_{238}	0.54	0.03
Quebrada Guaba bank	10.5	0.2	$\Gamma_{234}/\Gamma_{238}$	1.128	0.007
Sabana	11.7	0.3	$\Gamma_{230}/\Gamma_{234}$	0.022	0.003
w_{230}/w_{234} *set to 1*					
Sample ID	T_{res} (kyr)	2std.err.		value	2std.err.
RI-4	85	12	w_{238} (yr^{-1})	1.00E-05	8.3E-07
Icacos	5.4	0.3	w_{234}/w_{238}	1.100	0.002
Quebrada Guaba bed	22.1	0.8	Γ_{238}/k_{238}	0.19	0.08
Quebrada Guaba bank	12.1	0.3	$\Gamma_{234}/\Gamma_{238}$	1.341	0.013
Sabana	13.7	0.4	$\Gamma_{230}/\Gamma_{234}$	1.831	0.025

Table 4

Table 4. Solutions of the continuous loss-input nuclide model for Nunnock River

Suspended sediments					
w_{230}/w_{234} *set to* 10^{-10}					
Sample ID	T_w (kyr)	2std.err.		value	2std.err.
NUN01	443	10	w_{238} ($\times 10^{-5}$ yr^{-1})	1.60	0.04
NUN02	1423	88	w_{234}/w_{238}	1.114	0.003
NUN03	552	20	Γ_{238}/w_{238}	0.56	0.02
NUN04	1783	161	$\Gamma_{234}/\Gamma_{238}$	1.083	0.004
NUN05	1472	144	$\Gamma_{230}/\Gamma_{234}$	1.7E-10	4E-11
w_{230}/w_{234} *set to 0.5*					
Sample ID	T_w (kyr)	2std.err.		value	2std.err.
NUN01	346	12	w_{238} ($\times 10^{-5}$ yr^{-1})	0.92	0.05
NUN02	460	29	w_{234}/w_{238}	1.042	0.002
NUN03	378	29	Γ_{238}/w_{238}	0.13	0.01
NUN04	534	30	$\Gamma_{234}/\Gamma_{238}$	1.127	0.002
NUN05	1356	102	$\Gamma_{230}/\Gamma_{234}$	0.17	0.05

Bedload sediments					
w_{230}/w_{234} *and* $\Gamma_{230}/\Gamma_{234}$ *set to* 10^{-10}, *and* w_{234}/w_{238} *set to 1.05*					
Sample name	T_w (kyr)	2std.err.		value	2std.err.
NUN03	418	23	w_{238} ($\times 10^{-5}$ yr^{-1})	2.59	0.10
NUN04	407	21	Γ_{238}/w_{238}	0.22	0.01
NUN05	379	20	$\Gamma_{234}/\Gamma_{238}$	0.899	0.001
w_{230}/w_{234} *and* $\Gamma_{230}/\Gamma_{234}$ *set to* 10^{-10}, *and* w_{234}/w_{238} *set to 1.1*					
Sample name	T_w (kyr)	2std.err.		value	2std.err.
NUN03	439	21	w_{238} ($\times 10^{-5}$ yr^{-1})	1.17	0.05
NUN04	425	19	Γ_{238}/w_{238}	0.30	0.01
NUN05	393	18	$\Gamma_{234}/\Gamma_{238}$	0.927	0.001
w_{230}/w_{234} *and* $\Gamma_{230}/\Gamma_{234}$ *set to 0.5, and* w_{234}/w_{238} *set to 1.05*					
Sample name	T_w (kyr)	2std.err.		value	2std.err.
NUN03	478	19	w_{238} ($\times 10^{-5}$ yr^{-1})	1.60	0.05
NUN04	471	16	Γ_{238}/w_{238}	0.008	0.002
NUN05	453	17	$\Gamma_{234}/\Gamma_{238}$	0.894	0.001

Table 5

Table 5. List and values of parameters used to calculate weathering rates

Parameter	Unit	j = biotite	j = plag	Comments
a_j	$mol/m^2/yr$	$1.51x10^{-5}$	$1.09x10^{-5}$	Constant relating mineral dissolution rate to time (White and Brantley 2003)
α_j	unitless	-0.603	-0.564	Constant relating mineral dissolution rate to time (White and Brantley 2003)
b_j	unitless	13.6	13.6	Constant relating surface roughness to time (Yoo and Mudd 2008)
β_j	unitless	0.2	0.2	Constant relating surface roughness to time (Yoo and Mudd 2008)
ω_j	kg/mol	0.408	0.263	Mineral molar mass
D_j	m	0.0005	0.0005	Mineral particle diameter (Murphy et al., 1998; Buss et al., 2008)
$\rho_{\mu,j}$	kg/m^3	3000	2600	Mineral density
$X_{j,0}$	kg/kg	0.095	0.564	Initial mass fraction of mineral, Rio Icacos (White et al. 1998)
$X_{j,0}$	kg/kg	0.05	0.12	Initial mass fraction of mineral, Nunnock River (Burg and Wilson, 1988)
h	m	9	9	Weathering profile thickness, Rio Icacos (White et al. 1998)
h	m	30	30	Weathering profile thickness, Nunnock River (Green et al. 2006)

Table A1. Radionuclide data for Australian dust samples (Marx et al., 2005)

Sample ID	(^{226}Ra) (mBq/g)	±	U (ppm)	(^{230}Th) (mBq/g)	(^{226}Ra/^{230}Th)	±
Red Fox Dust 00	15	2	1.912	26.15	0.57	0.11
Grey Fox 03	12	2	2.49	34.06	0.35	0.07
Brown Fox Lower 04	14	1	2.449	33.49	0.42	0.08
Grey fox lower 04	11	1	1.891	25.86	0.43	0.09
Fox glacier millk	11	1	1.92	26.26	0.42	0.08
Red fox april 04	22	2	2.184	29.87	0.74	0.15
Cleve	17	1	1.929	26.38	0.64	0.13
Wilcannia	11	1	1.377	18.83	0.58	0.12
Buronga	15	1	0.723	9.89	1.52	0.30
Lake Menindee	15	2	1.545	21.13	0.71	0.14
Lake Eyre	10	1	1.338	18.30	0.55	0.11

^{230}Th activity and (^{226}Ra/^{230}Th) are calculated assuming a (^{230}Th/^{238}U) activity ratio of 1.1 ± 0.1 (as ^{230}Th was not measured in Marx et al. (2005)). Errors on (^{226}Ra) activity as reported in Marx et al. (2005). Errors on (^{226}Ra/^{230}Th) are calculated by propagating errors on (226Ra) and on the assumed (^{230}Th/^{238}U) ratio.

Table A2. Thorium isotope data for regolith samples from the LG1 weathering profile

Sample name	Depth (m)	Type	(^{230}Th/^{232}Th)
LG1 -0.5ft	0.1	A soil	1.692
LG1 -1ft	0.3	B soil	1.659
LG1 -1.5ft	0.5	B soil	1.816
LG1 -2ft	0.6	B soil	1.819
LG1 -3ft	0.9	B soil	1.891
LG1 -3.5ft	1.1	saprolite	0.929
LG1 -5ft	1.5	saprolite	1.173
LG1 -6ft	1.8	saprolite	1.556
LG1 -7ft	2.1	saprolite	1.923
LG1 -8ft	2.4	saprolite	1.367
LG1 -10ft	3.0	saprolite	1.680
LG1 -12ft	3.7	saprolite	1.787
LG1 -13ft	4.0	saprolite	1.491
LG1 -15ft	4.6	saprolite	1.337
LG1 -16ft	4.9	saprolite	1.356
LG1 -17ft	5.2	saprock	1.195
LG1 -18ft	5.5	saprock	1.187
LG1 -19ft	5.8	saprock	0.619
LG1 -20ft	6.1	saprock	0.808
LG1 -20ft *replicate*	6.1	saprock	1.063
LG1 -23ft	7.0	saprock	0.839

Relative external analytical uncertainty for (^{230}Th/^{232}Th) ratios is 13.6%, based on replicate analysis of sample LG1-20ft (1 standard deviation).

Table A3. Upper and lower boundaries of variables using in the weathering age model

	Upper value	Lower value
Weathering age, T_w (yr)	100	1,000,000
w_{238} (yr^{-1})	10^{-3}	10^{-8}
w_{234}/w_{238}	1	5
Γ_{238}/w_{238}	10^{-8}	10^{3}
$\Gamma_{234}/\Gamma_{238}$	0.1	10
$\Gamma_{230}/\Gamma_{234}$	10^{-12}	10^{5}

Table A4. Trace element data (in ppm)

Sample name	*Puerto Rico*	RI-1 >25 μm	RI-2 bed sediments	RI-3 bed sediments	RI-4 bed sediments	RI-5 bed sediments	RI-6 >25 μm	RI-6 bed sediments	RI-7 >25 μm	RI-7 bed sediments	RI-7 bank sediments	*Australia*	NUN03 bed sediments	NUN04 bed sediments	NUN05 bed sediments
Li		12.9	12.5	13.9	7.8	5.5	14.2	10.4	12.8	8.6	11.1		8.3	9.3	8.4
Be		0.7	1.4	1.1	0.5	0.7	1.0	0.4	1.2	0.4	0.6		0.8	1.4	1.6
Sc		10.8	33.7	22.4	12.2	6.5	16.9	9.8	18.5	14.5	10.9		1.8	3.8	3.2
Ti		2504	6223	3563	1670	2372	4024	2137	3201	2878	2812		396	615	565
V		79.9	302.5	189.6	104.6	128.8	109.2	78.3	85.6	232.0	75.6		7.5	13.4	13.7
Cr		5.0	23.4	101.9	16.8	10.8	14.4	5.1	9.9	8.8	3.7		2.3	3.4	5.1
Co		11.9	18.8	24.4	16.6	4.8	20.9	12.6	16.3	12.9	13.8		1.6	1.7	1.5
Ni		4.0	8.0	42.4	6.7	2.3	24.5	2.9	5.7	3.5	3.0		1.1	1.5	3.5
Cu		35.5	37.5	129.0	12.0	30.4	132.5	30.1	87.7	29.8	54.6		1.5	3.7	3.0
Zn		175.8	70.2	100.3	38.3	24.6	547.2	39.8	327.9	50.7	53.9		12.2	15.0	13.1
Ga		9.4	34.9	25.0	5.9	8.4	13.4	6.0	18.4	7.4	10.4		5.8	8.1	9.1
As		2.0	2.0	1.8	1.8	2.2	2.2	1.8	2.0	1.8	1.9		2.0	1.8	1.8
Rb		27.7	69.1	13.6	8.6	9.3	37.7	16.7	41.7	21.8	42.1		79.1	88.8	104.3
Sr		53.4	157.7	206.7	79.1	206.0	62.0	32.4	76.6	42.7	51.5		26.2	75.9	91.2
Y		16.9	93.4	21.1	14.6	8.8	20.3	12.4	29.1	21.2	19.2		4.3	8.4	7.0
Zr		12.7	7.9	53.8	6.0	4.3	15.5	5.2	12.0	8.3	6.3		18.0	22.0	22.2
Nb		2.1	3.3	3.1	1.0	1.8	3.0	1.3	2.5	1.6	2.2		1.4	2.1	2.0
Mo		0.4	1.3	2.3	0.3	0.6	1.0	0.3	0.4	0.5	0.3		0.1	0.1	0.1
Rh		148.7	139.9	136.5	141.8	173.7	165.3	143.0	156.4	135.0	147.3		163.9	144.7	148.0
Cd		0.12	0.06	0.22	0.03	0.03	1.91	0.03	0.21	0.04	0.04		0.04	0.07	0.03
In		148.0	160.6	136.6	139.0	170.0	163.7	139.3	157.1	133.8	145.4		158.5	142.2	144.9
Sn		0.9	0.8	2.1	0.7	0.6	6.0	1.5	4.1	1.2	1.9		12.3	18.7	4.5
Sb		0.14	2.86	0.72	0.08	0.44	0.59	0.09	0.14	0.15	0.08		0.13	0.17	0.19
Cs		1.5	1.9	0.7	0.6	0.4	2.5	1.1	2.5	0.9	2.0		2.3	2.7	2.9
Ba		264	1420	1187	149	258	325	190	455	233	385		269	350	392
La		5.8	14.3	13.1	3.5	5.4	10.3	3.7	8.5	4.6	6.9		3.2	5.1	5.1
Ce		13.5	21.1	20.9	10.4	10.6	18.8	9.4	18.6	11.8	12.2		5.8	8.7	10.4
Pr		2.1	4.9	4.0	1.4	1.4	2.8	1.4	2.8	1.9	2.3		0.8	1.3	1.2
Nd		9.0	22.8	16.9	6.3	5.6	11.9	6.5	12.5	8.8	9.8		3.1	4.8	4.4
Sm		2.3	6.9	4.0	1.8	1.3	3.0	1.7	3.3	2.5	2.4		0.7	1.1	1.0
Eu		0.70	2.46	1.26	0.55	0.57	0.99	0.51	1.08	0.59	0.80		0.28	0.57	0.61
Gd		2.4	9.6	3.9	2.1	1.4	3.1	1.9	3.7	2.7	2.6		0.6	1.2	1.0
Tb		0.40	1.80	0.60	0.37	0.22	0.50	0.32	0.65	0.48	0.43		0.11	0.21	0.17
Dy		2.5	11.6	3.5	2.3	1.4	3.1	2.0	4.2	3.1	2.7		0.7	1.3	1.1
Ho		0.55	2.61	0.72	0.52	0.30	0.67	0.44	0.94	0.69	0.61		0.15	0.29	0.24
Er		1.6	7.3	2.0	1.6	0.9	2.0	1.3	2.8	2.1	1.8		0.5	0.9	0.7
Tm		1.8	1.8	1.7	1.7	2.0	2.1	1.6	2.0	1.7	1.8		1.7	1.6	1.7
Yb		1.7	5.6	2.0	1.6	1.0	2.0	1.3	3.0	2.1	1.8		0.5	0.9	0.7
Lu		0.28	0.84	0.29	0.25	0.15	0.32	0.21	0.47	0.33	0.29		0.08	0.13	0.11
Hf		0.63	0.43	1.73	0.39	0.25	0.67	0.31	0.73	0.53	0.41		0.69	0.85	0.80
Ta		0.14	0.17	0.20	0.06	0.10	0.20	0.08	0.19	0.11	0.14		0.17	0.20	0.20
W		1.7	22.0	3.4	0.6	0.7	2.2	0.8	1.9	0.6	0.9		0.6	1.1	0.6
Pb		4.8	6.2	6.0	3.6	2.3	19.2	2.7	6.7	2.3	3.2		6.1	8.4	8.7
Bi		2.0	2.0	1.8	1.8	2.2	2.3	1.8	2.1	1.8	1.9		2.0	1.8	1.9

Figures

Figure 1

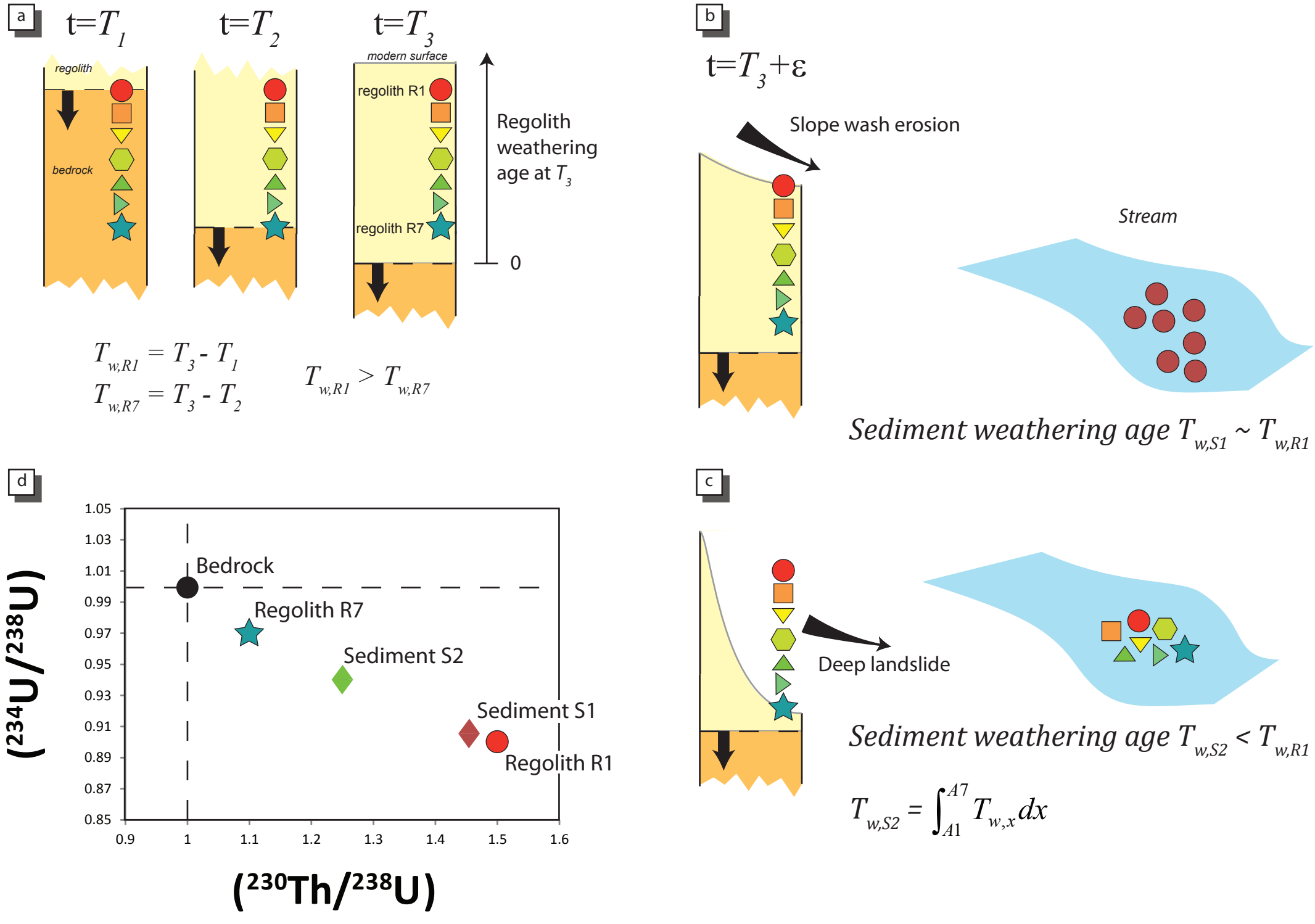

Figure 2

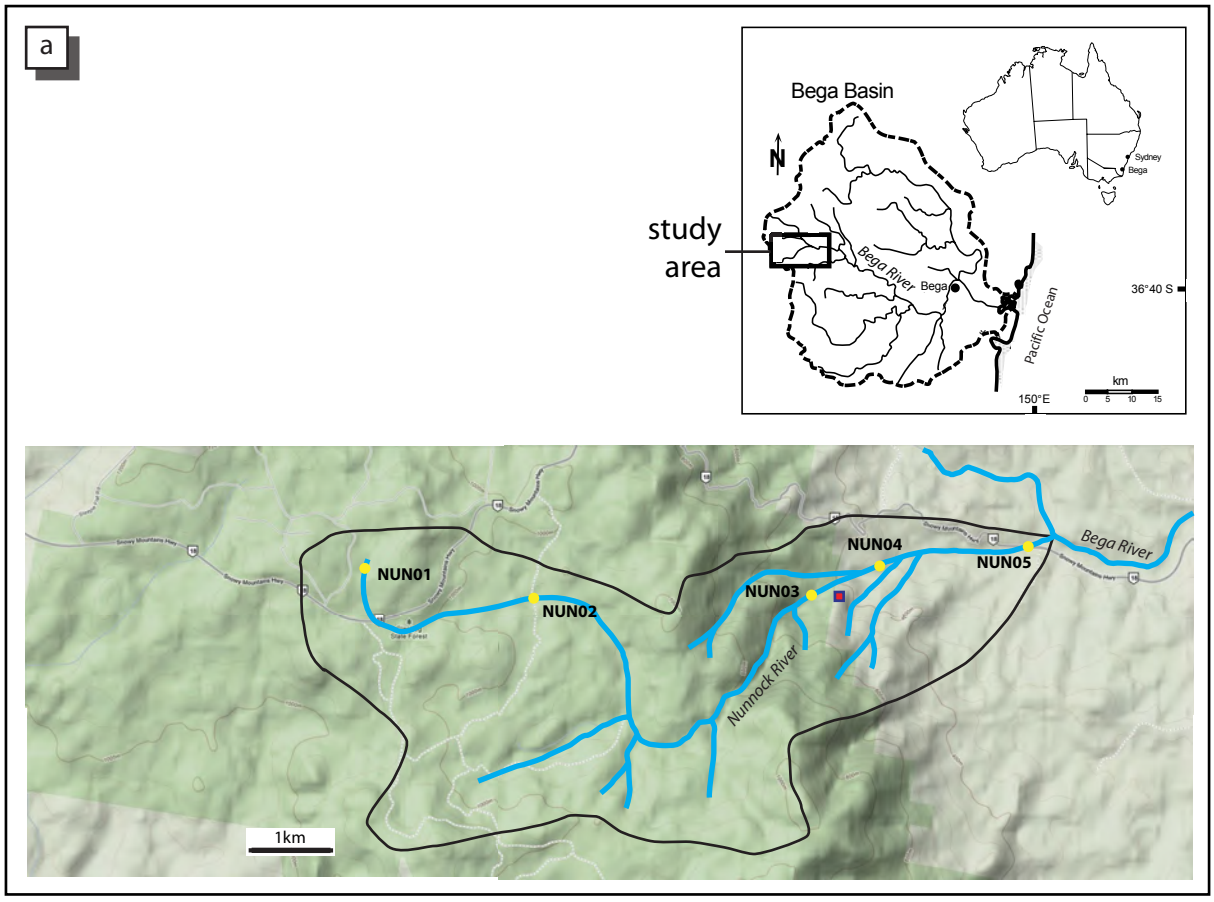
a
Bega Basin
N
study
area
Bega River
Bega
Pacific Ocean
36°40 S
150°E
km
0 5 10 15
Sydney
Bega
NUN01
NUN02
NUN03
NUN04
NUN05
Bega River
Nunnock River
1km

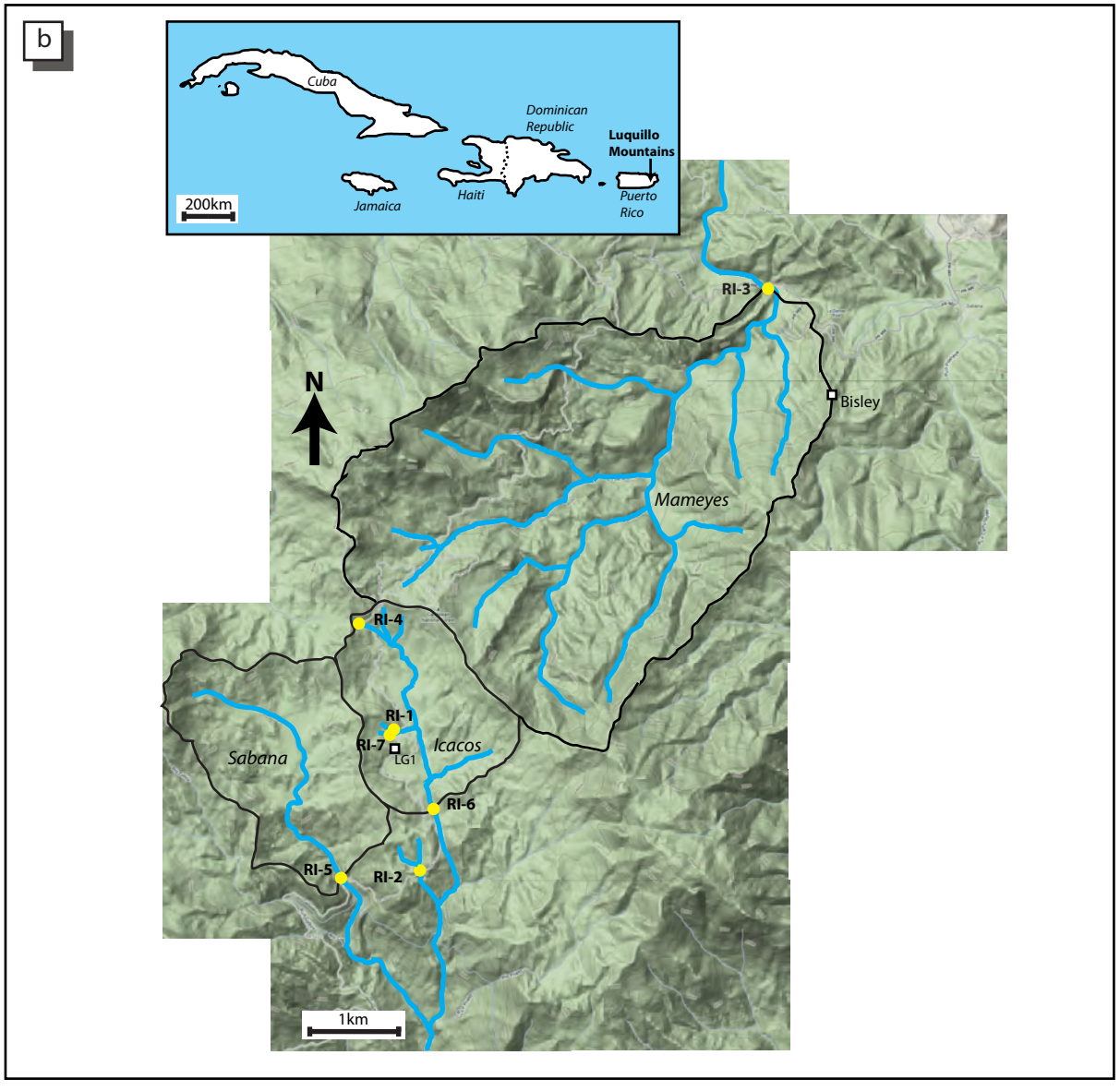
b
Cuba
Dominican
Republic
Luquillo
Mountains
Haiti
Jamaica
Puerto
Rico
200km
N
RI-3
Bisley
Mameyes
RI-4
RI-1
RI-7
LG1
Icacos
Sabana
RI-6
RI-5
RI-2
1km

Figure 3

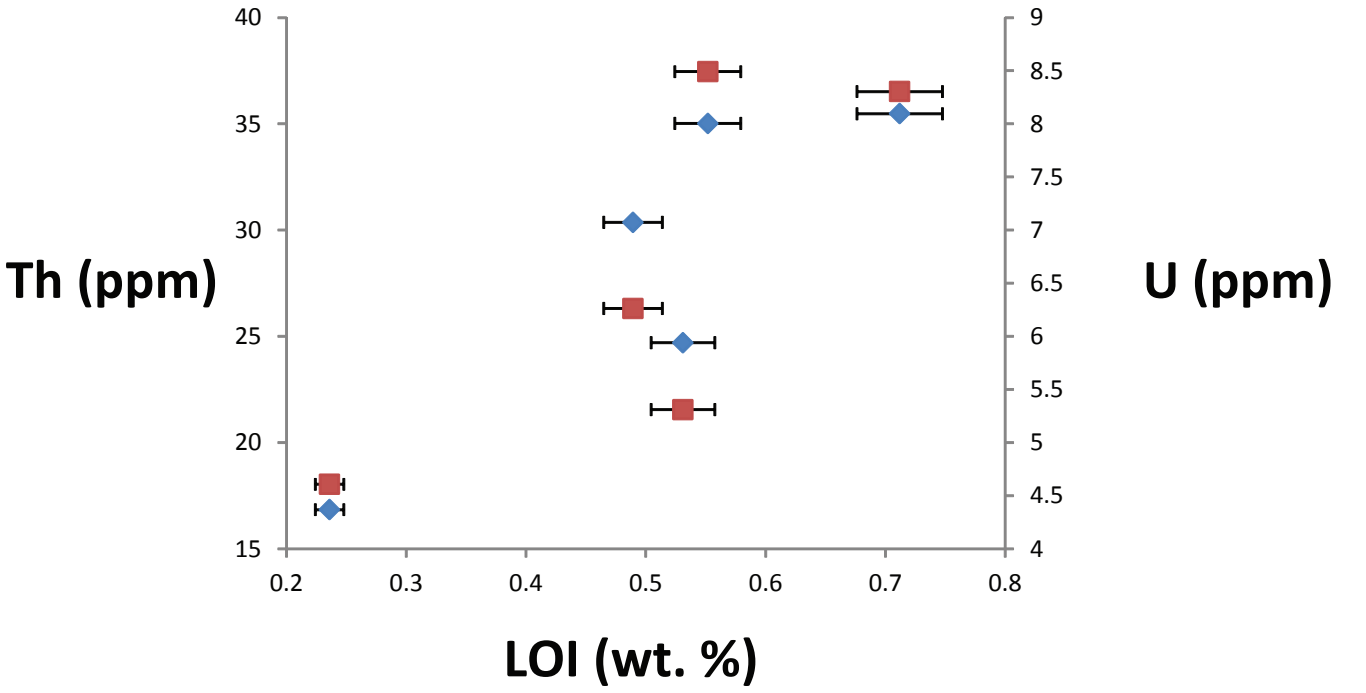
Th (ppm)
U (ppm)
LOI (wt. %)
40
35
30
25
20
15
9
8.5
8
7.5
7
6.5
6
5.5
5
4.5
4
0.2
0.3
0.4
0.5
0.6
0.7
0.8

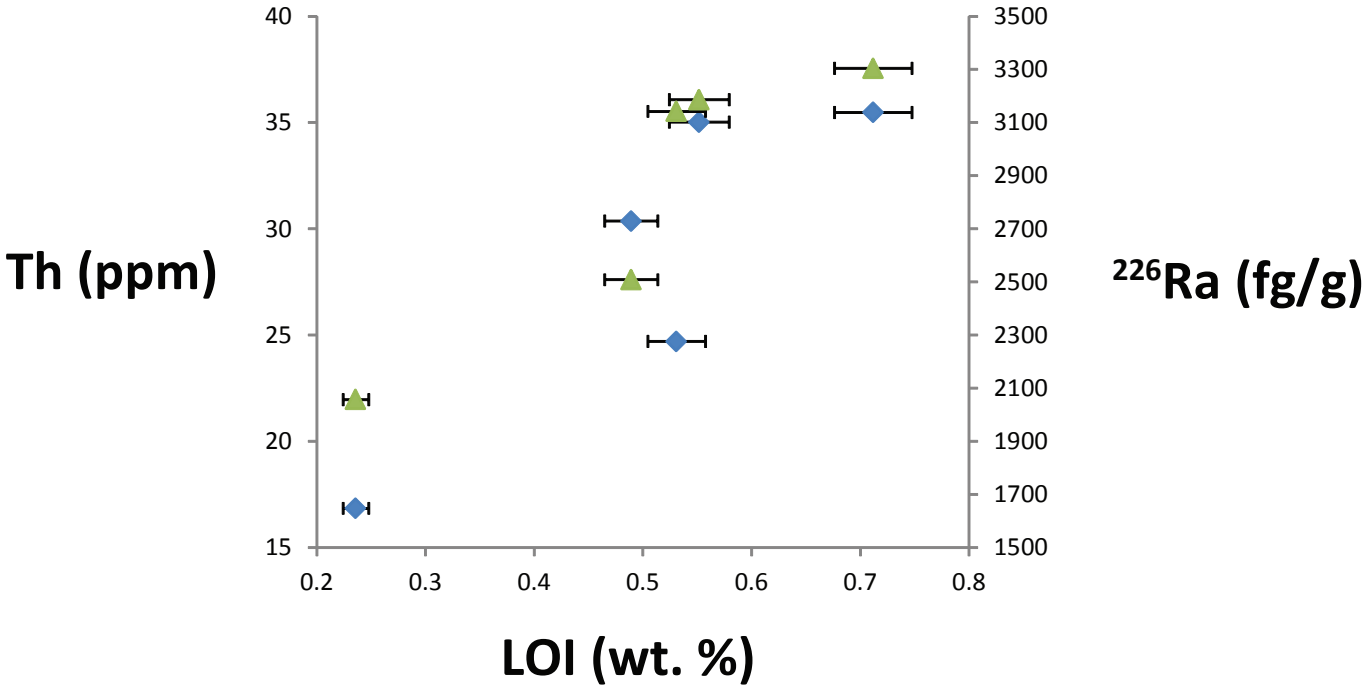
Th (ppm)
226Ra (fg/g)
LOI (wt. %)
40
35
30
25
20
15
3500
3300
3100
2900
2700
2500
2300
2100
1900
1700
1500
0.2
0.3
0.4
0.5
0.6
0.7
0.8

Figure 4

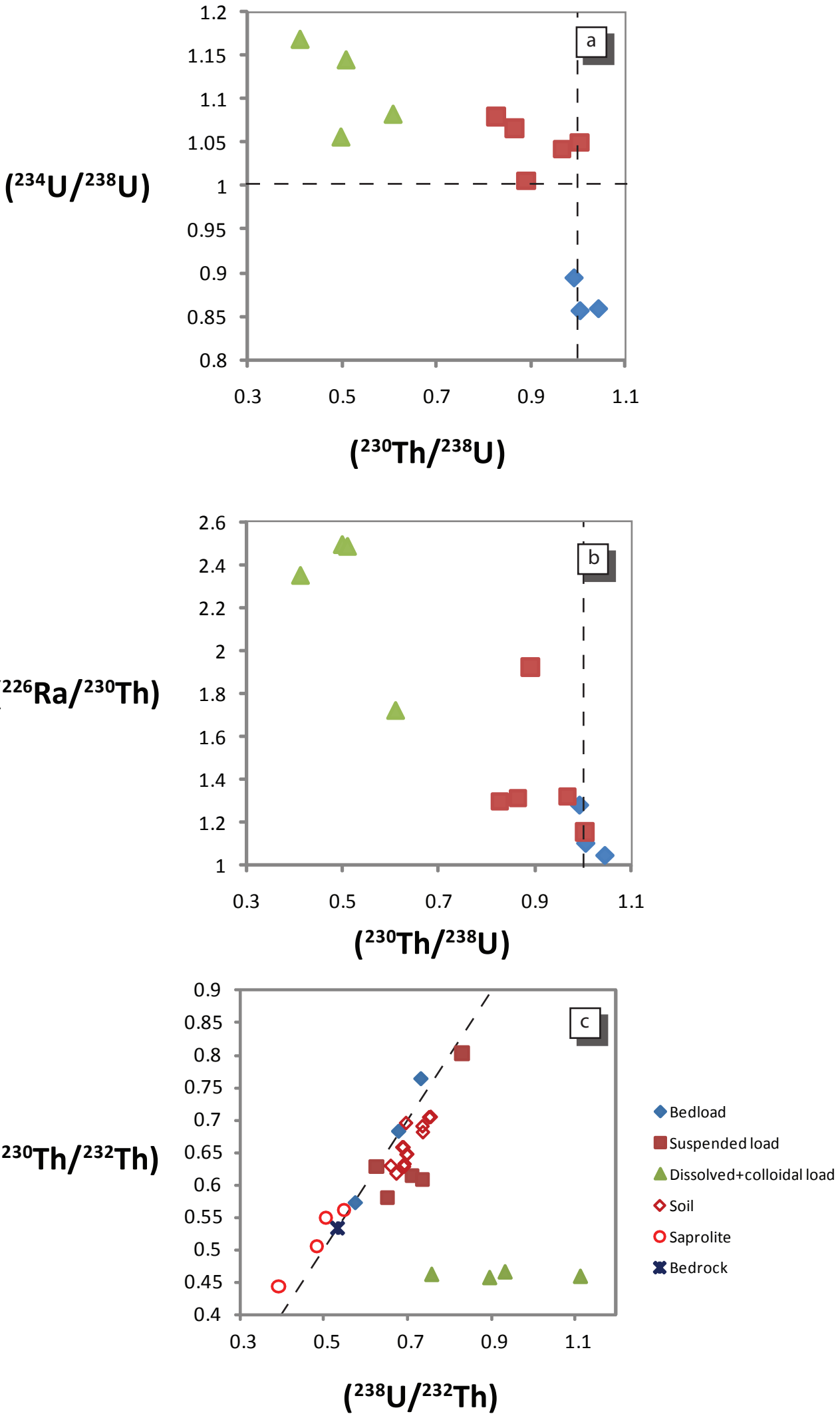
a
(234U/238U)
1.2
1.15
1.1
1.05
1
0.95
0.9
0.85
0.8
0.3
0.5
0.7
0.9
1.1
(230Th/238U)
b
(226Ra/230Th)
2.6
2.4
2.2
2
1.8
1.6
1.4
1.2
1
0.3
0.5
0.7
0.9
1.1
(230Th/238U)
c
(230Th/232Th)
0.9
0.85
0.8
0.75
0.7
0.65
0.6
0.55
0.5
0.45
0.4
0.3
0.5
0.7
0.9
1.1
(238U/232Th)
Bedload
Suspended load
Dissolved+colloidal load
Soil
Saprolite
Bedrock

Figure 5

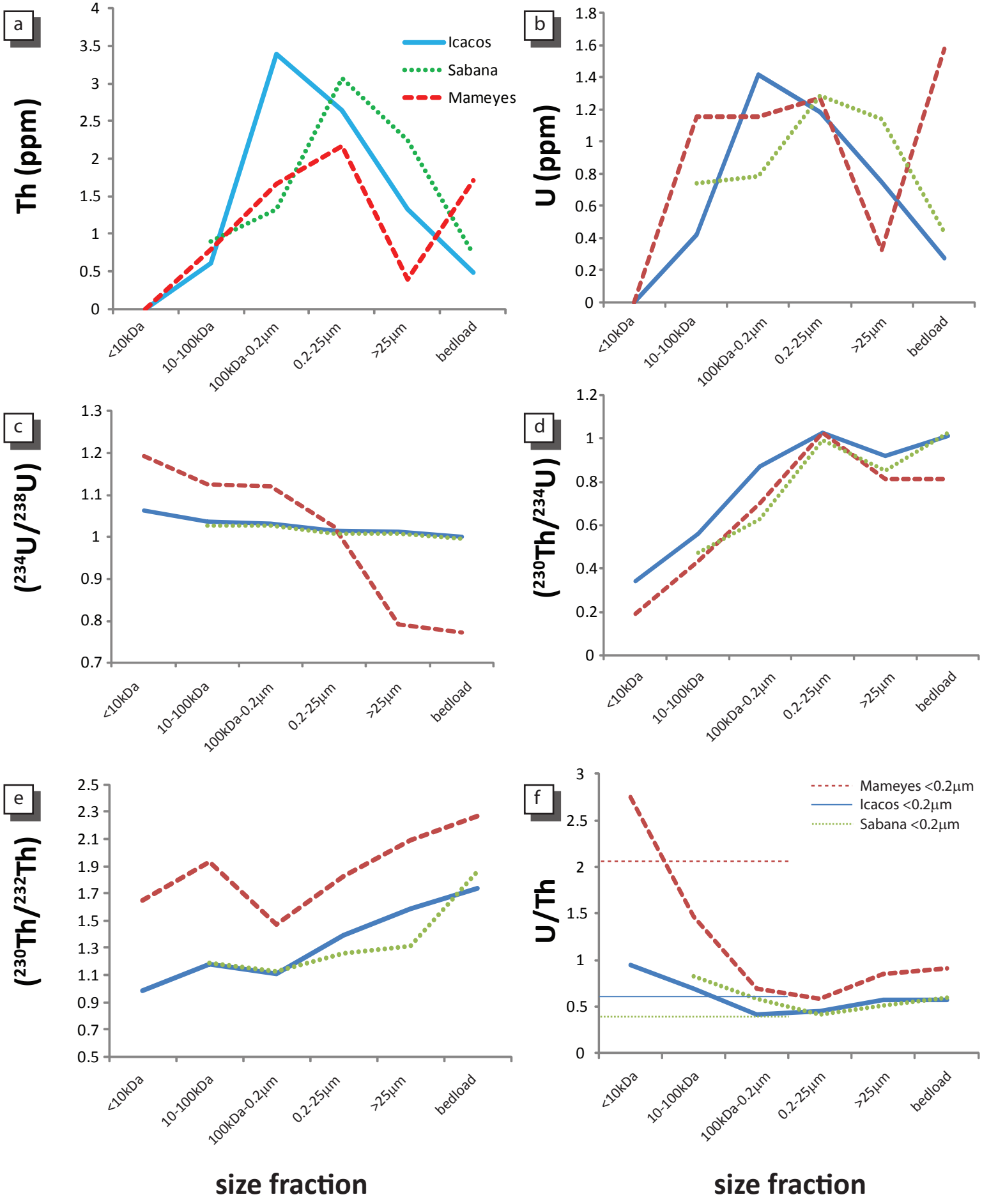
a
Th (ppm)
Icacos
Sabana
Mameyes
b
U (ppm)
c
(234U/238U)
d
(230Th/234U)
e
(230Th/232Th)
f
U/Th
Mameyes <0.2µm
Icacos <0.2µm
Sabana <0.2µm
<10kDa
10-100kDa
100kDa-0.2µm
0.2-25µm
>25µm
bedload
size fraction
size fraction

Figure 6

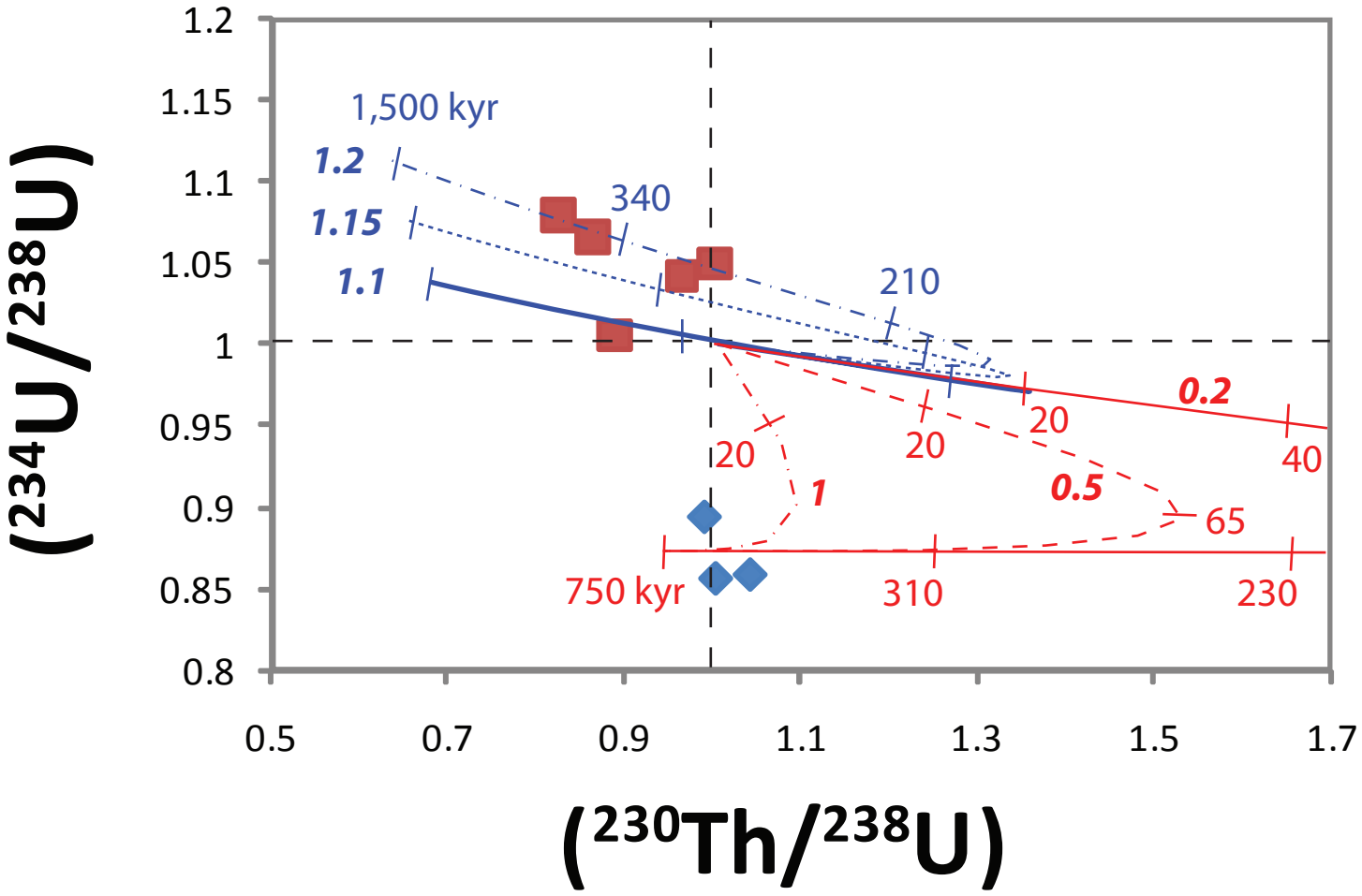
1.2
1.15
1.1
1.05
1
0.95
0.9
0.85
0.8
0.5
0.7
0.9
1.1
1.3
1.5
1.7
(234U/238U)
(230Th/238U)
1,500 kyr
1.2
1.15
1.1
340
210
0.2
20
20
20
40
1
0.5
65
750 kyr
310
230

Figure A1